Integrated Silicon Field-Effect Sensors and Microfluidics for Biomolecular Detection

by

Peter R. Russo

Submitted to the Department of Electrical Engineering and Computer Science
in Partial Fulfillment of the Requirements for the Degree of
Master of Engineering in Electrical Engineering and Computer Science
at the Massachusetts Institute of Technology
February 9, 2004

Author____
Department of Electrical Engineering and Computer Science
February 9, 2004

Certified by__ ________________
Scott R. Manalis
Thesis Supervisor

Accepted by__________ ________________
Arthur C. Smith
Chairman, Department Committee on Graduate Theses

Integrated Silicon Field-Effect Sensors and Microfluidics for Biomolecular Detection
by
Peter R. Russo

Submitted to the
Department of Electrical Engineering and Computer Science

February 9, 2004

In Partial Fulfillment of the Requirements for the Degree of
Master of Engineering in Electrical Engineering and Computer Science.

ABSTRACT

Microfabricated silicon field-effect sensors with integrated poly(dimethylsiloxane) microfluidic channels have been demonstrated. These devices are designed for the label-free detection and recognition of specific biomolecules such as DNA. Label-free methods eliminate the time-consuming and costly step of tagging molecules with radioactive or fluorescent markers prior to detection. The devices presented here are sensitive to the intrinsic charge of the target molecules, which modulates the width of the carrier-depleted region of a lightly-doped silicon sensor. The variable depletion capacitance is precisely measured, indicating changes in sensor surface potential of less than 30μV. The integrated microfluidic channels enable the delivery of small (nanoliter-scale) amounts of fluid directly to the sensors. Capacitance-voltage curves were recorded using phosphate buffered saline (PBS) as the test electrolyte; a maximum slope of 44pF/V was measured in depletion. pH sensitivity was also demonstrated using modified PBS solutions. A device with dual 80x80μm sensors yielded a response of 40mV/decade, referenced to the fluid electrode. A device with dual 50x50μm sensors yielded a response of 12mV/decade, referenced to the sensors.

Thesis Supervisor: Scott R. Manalis
Title: Associate Professor, Program in Media Arts and Sciences

ACKNOWLEDGEMENTS

I would like to first thank my advisor, Prof. Scott Manalis, for introducing me to the world of microfabrication and MEMS while I was an undergraduate, and for setting me up with a terrific M.Eng. research project. The past two and a half years working with Scott have been tremendously rewarding.

My fellow Nanoscale Sensing Group colleagues, Dr. Paul Ashby, Thomas Burg, Dr. Emily Cooper, Dr. Jürgen Fritz, Shelly Levy-Tzedek, Nin Loh, Dr. Cagri Savran, Maxim Shusteff, and Andrew Sparks, have been an amazing group to work with. Emily, in particular, has provided numerous technical insights on the intricacies of field-effect detection, and Nin spent countless hours teaching me the ins and outs of the fab during summer 2001.

Without the efforts of my classmates in the spring 2002 Semiconductor Devices Project Laboratory, Daniel Bedard, Antimony Gerhardt, Trisha Montalbo, Maxim Shusteff, and Luke Theogarajan, this project may never have gotten off the ground. Our co-advisor in the class, Prof. Martin Schmidt, has also provided very helpful guidance along the way.

The contribution of the M.I.T. Microsystems Technology Laboratories staff, particularly Vicky Diadiuk, Kurt Broderick, and Paul Tierney, has been invaluable. Without their process development help and technical assistance, the devices discussed in this thesis could not have been built.

This research has been funded by the NSF Center for Bits and Atoms and the Hewlett-Packard corporation.

And finally I thank my family for supporting me in all of my endeavors, particularly my education.

TABLE OF CONTENTS

LIST OF FIGURES

LIST OF TABLES

1. INTRODUCTION

1.1 Label-free biosensors and field-effect detection

Many sensors that currently exist for biomolecular detection rely on the labeling of target molecules with fluorescent, radioactive, or other types of labels. While these methods are very sensitive to a small number of molecules, they have significant limitations. First, the tagging of target molecules can be a lengthy and expensive process, as it adds extra steps to detection assays. Second, complex equipment (for example, a microscope, UV light source, and CCD camera in the case of fluorescence labeling) is necessary for the readout of results, making these methods best suited for a laboratory environment. The recent development of label-free electrical and mechanical methods is eliminating the need for tagging target molecules and the complex equipment necessary for readout, enabling faster, cheaper, and more portable detection. A disadvantage of label-free detection is a loss in sensitivity when compared to label-dependent methods, although the sensitivity of label-free detection is rapidly improving.

One label-free method currently under investigation is field-effect detection. A field-effect biosensor is essentially a metal-oxide-semiconductor (MOS) capacitor whose metal gate has been replaced with an electrolyte, thus forming an electrolyte-insulator-semiconductor (EIS) structure. While MOS and EIS technology has been around for many years, only recently has it been used specifically for biodetection. In fact, there are many applications for field-effect biosensors. First, they may be used to detect changes in the pH of a solution. In experiments described in [15], a field-effect sensor on the tip of a cantilever is moved through a pH gradient. The amount of surface charge at the gate insulator changes with the pH, as pH is a measure of relative H+ and OH- concentrations in solution.

Another application is the detection of DNA. In experiments described in [4, 9], positively charged poly-L-lysine (PLL) molecules are applied to the sensor surface, to which negatively charged DNA probes are attached. Complementary target DNA is then applied to the sensor, which binds to the probes. The presence of the bound target DNA may be detected due to its negative intrinsic charge. Other biological mechanisms such as protein binding are also being actively pursued for possible field-effect detection.

1.2 Problem description

The field-effect sensors previously developed in the Manalis lab at M.I.T. (designed by Fritz, Cooper, et al.; see [4], [9], [15]) are microfabricated at the tips of cantilevers, and are intended for the insertion into a enclosed fluid cell. The sensors are well isolated electrically, as the silicon-on-insulator (SOI) fabrication process mechanically separates the sensors from each other, and the fluid reference electrode is external.

There are several limitations to these sensors, however. The primary limitation is that the sensors are delivered to a relatively large volume of fluid (perhaps 500μL [9]) which is contained in a bulky fluid cell. Once the solution is inside the fluid cell, it is impossible to quickly replace it with another solution. It is also difficult to split that fluid into multiple parts, in order to run separate experiments on each part (which may be necessary if only a small amount of fluid is initially available, a common problem when dealing with biological systems). Furthermore, these sensors may not readily be integrated into a micro total analysis system (μ-TAS). A μ-TAS may combine several processing steps on a single chip-sized module, such as DNA concentration, filtering, and detection.

The design goal for the current research is to develop a flat field-effect sensor chip, with integrated microfluidic handling. Rather than delivering sensors to a bulky fluid cell, a much smaller amount of fluid is delivered directly to the sensors. The microfluidics must be precisely aligned to the silicon chip, in order for fluid to reach the sensors. A fluid reference electrode must also be integrated into the system, as will be explained in section 2.2.

1.3 Thesis overview

In this document, the design, fabrication, packaging, and testing of a sensor chip with integrated microfluidics will be presented. Chapter 2 discusses the basic theory behind the detection method used by the chip. Chapter 3 describes the design process in detail, including the basic device structure, the evolution of previous sensors, process development, and simulation results. The fabrication and packaging of the silicon sensor chip and the integrated microfluidics are described in chapter 4. The testing procedures and measurement results are presented in chapter 5. Dry measurements, used for device characterization, and wet measurements using electrolyte buffer are both discussed. Chapter 6 provides a brief summary of the work that has been done, as well as future directions of study that are being planned for the devices. Detailed fabrication notes, full SUPREM simulation code, and discussion of air-actuated microfluidic valves are included in the appendices.

2. THEORY

2.1 MOS capacitors and the depletion regime

The theory behind field-effect biomolecular sensing may be understood by examining the operation of a metal-oxide-semiconductor (MOS) capacitor. In a MOS capacitor, a thin dielectric film (usually SiO_2) separates a topside metal gate from silicon on the bottom. If the silicon is p-type and sufficient positive charge is applied to the gate, the majority-carrier holes in the silicon will be repelled, creating a carrier-depleted region. If too little positive charge is applied, the p-type carriers will not be repelled, and the capacitor will be in the accumulation regime. If too much positive charge is applied, electrons will migrate up to the silicon-dielectric interface, inverting the silicon to n-type near the surface. The most interesting regime of operation for biological detection purposes, depletion, lies in between accumulation and inversion. In depletion, small changes in gate charge (V_{GB}) will vary the width of the carrier-depleted region (x_d) as

$$x_d = t_{ox}\frac{\varepsilon_S}{\varepsilon_{ox}}\left(\sqrt{1+\frac{2C_{ox}^2(V_{GB}-V_{FB})}{q\varepsilon_S N_a}}-1\right)$$

where t_{ox} is the thickness of the gate dielectric, ε_s and ε_{ox} are the respective dielectric constants for silicon and SiO_2, V_{FB} is the flatband voltage, and N_a is the majority-carrier concentration in the p-type silicon [12]. All of the terms in this equation are constant except for the applied gate bias, V_{GB}.

A depletion capacitance arises essentially as a parallel-plate capacitor with dielectric thickness equal to the depletion width, and dielectric constant equal to that of silicon:

$$C_{dep} = \frac{\varepsilon_{si}}{x_d}$$

The total capacitance across the gate oxide and the depletion region is approximately

$$C_{tot} = \left(\frac{1}{C_{ox}} + \frac{1}{C_{dep}} \right)^{-1} = \left(\frac{1}{\frac{\varepsilon_{ox}}{t_{ox}}} + \frac{1}{\frac{\varepsilon_{si}}{x_d}} \right)^{-1}$$

Because C_{ox} is purely a function of the SiO_2 thickness, which is constant, C_{tot} varies only with C_{dep}.

2.2 Electrolyte-Insulator-Semiconductor devices

In an electrolyte-insulator-semiconductor (EIS) device used for biosensing, the metal gate of the MOS capacitor is replaced with an electrolytic solution. The structure still otherwise consists of a thin dielectric film separating the electrolyte from a silicon region. Now instead of applying charge to a metal gate to modulate the width of the depletion region in the silicon, the depletion region is modulated by the surface potential at the SiO_2 interface, which varies with the presence of charged molecules in the electrolyte. The amount and type of charged molecules may be a function of the electrolyte pH value, or the presence of biological materials such as DNA, which carries a negative intrinsic charge. To be detected, the charge must be within a Debye length of the SiO_2 surface. The Debye length is calculated as

$$\frac{1}{\kappa} = \sqrt{\frac{\varepsilon RT}{2z^2F^2c}}$$

where ε is the solution permittivity, R is the universal gas constant, T is temperature, z is the ionic strength of the solution, F is the Faraday constant, and c is the concentration of solutes in solution [5]. Molecules farther then one Debye length away from the SiO_2 surface will be screened by mobile counter ions in the solution. As the ionic strength of the electrolyte increases, more charged molecules arescreened, and the Debye length decreases. A typical Debye length for biological-strength buffers is 1-10nm [1, 5].

To measure the depletion capacitance, and thus obtain information about the SiO_2 surface potential, a small-signal voltage sine wave is applied to the fluid with a reference electrode. AC current flow from the electrode to the silicon is measured. The relationship between the applied voltage, the measured current, and the depletion capacitance, is described by Ohm's Law:

$$V_{rms} = I_{rms} \cdot |Z_C|$$

where V_{rms} is the root-mean-square voltage of the applied sine wave, I_{rms} is the root-mean-square current flowing into the silicon, and $|Z_C|$ is the magnitude of the complex impedance of C_{tot}. The complex impedance is a function of C_{tot} and frequency ω:

$$Z_C = \frac{1}{j\omega C_{tot}}$$

Thus, by knowing V_{rms} and measuring I_{rms}, C_{tot} may be determined:

$$C_{tot} = \frac{I_{rms}}{V_{rms} \cdot \omega}$$

It should be noted that C_{tot} is an approximation; several other sources contribute to C_{tot}, such as double-layer capacitance in the electrolyte [6]. However, for the scope of this research, C_{tot} is just considered to be a function of C_{ox} and C_{dep}.

For biolomolecular detection, rather than measuring absolute capacitance values, it is most useful to detect small incremental capacitance changes. Thus, the devices are DC biased (either with the fluid reference electrode or at the sensors) to their most sensitive operating points, where modulation of surface charge results in the maximum change in depletion width. Experiments are then performed around this bias point, and incremental capacitance changes are amplified and measured.

3. DESIGN

3.1 Basic device structure

The basic concept for the integrated field-effect sensors and microfluidics consists of two separately fabricated modules which are aligned and bonded together: a silicon sensor chip, and a poly(dimethylsiloxane) microfluidics module. The microfluidic channels move solutions around on top of the chip, while structures built into the silicon perform field-effect detection of charged molecules in the solution. The sensor chip is made using traditional microfabrication methods, such as photolithography, etching, and ion implants, while the fluid channels are made with a relatively straightforward replica molding technique.

The sensor chip that has been developed consists of lightly-doped p-type sensor regions implanted in an n-type substrate. The sensors are insulated from the fluid by a thin dielectric film (SiO_2), as described in section 2.2. Charged molecules in the solution modulate the depletion width in the sensor areas. Highly-doped p+ conductive traces implanted in the substrate connect to the sensor regions. With the exception of the sensor areas, the chip is passivated with a thick field dielectric (Si_3N_4), which insulates the fluid from the underlying silicon, such that only charged molecules at the sensor locations may be detected. In addition to the thick field dielectric, the field areas are highly-doped n+, providing a conductive ground plane over which the topside metal traces run, reducing capacitive coupling. The metal traces connect to the p+ conductive traces via contact holes that are etched in the field dielectric. A metal reference electrode applies a small-signal sine wave to the fluid, as described in section 2.2. As with the sensors, a highly-conductive p+ trace connects to the electrode.

3.2 Device evolution

The first generation of integrated silicon field-effect sensors and microfluidic channels [1] was fabricated during spring 2002 for the Semiconductor Devices Project Laboratory class at M.I.T. Our device included two sensors that fit side-by-side in a 100μm wide fluid channel. The main problem encountered with these devices was a short lifetime. After a short period of wet testing with electrolyte solution (during which they would yield capacitance-voltage curves as expected), the devices would fail; CV curves no longer had the proper shape, and signal amplitude would drop dramatically. There were also design choices that limited the operation of the sensors. For example, the close proximity of the two sensors made it impossible to isolate them effectively from each other and from the integrated gold bias electrode.

These first generation sensors were fabricated on 4-inch wafers using low-resolution (5,080 dpi) transparency photomasks. While edges were quite rough, and small features were misshapen, the alignment precision across the 4-inch wafers was generally acceptable for the critical feature size (approximately 25μm).

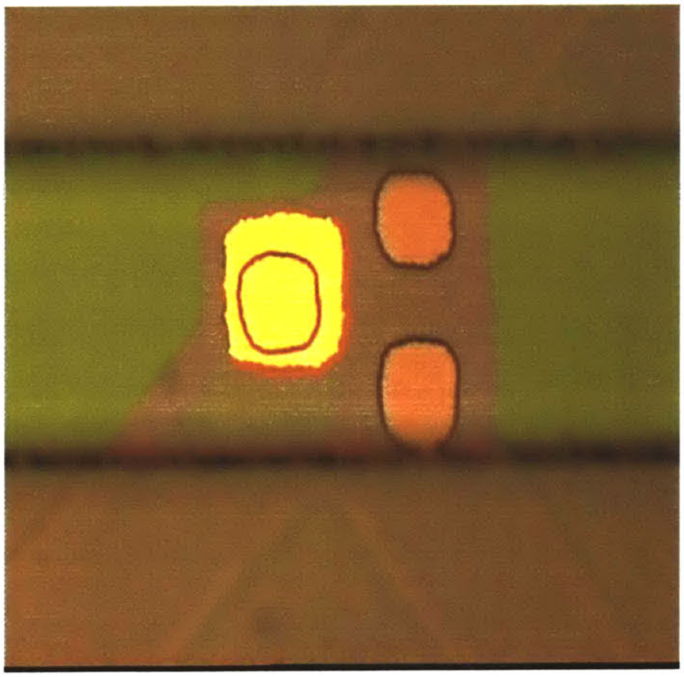

Fig. 3.1: Close-up of a first-generation device fabricated during 6.151, showing fluid reference electrode (left) and two sensor regions. Channel width is 100μm.

The second generation sensors were fabricated during fall 2002 as part of the research for this thesis project. These devices were again patterned using low-resolution transparency photomasks, but on 6-inch substrates. Across a 6-inch diameter, the alignment precision proved to be inadequate for 25μm features. In particular, contact holes to the implanted traces were badly aligned, and they often contacted the substrate as well, effectively shorting all of the traces together when metal was deposited into the holes. The sensor areas were patterned with a chrome mask, but it was difficult to align it to the transparency-patterned registration marks. Alignment was so poor that it was difficult to determine whether or not the lightly-doped p sensor implants even contacted the p+ connecting traces. During the testing of some devices, it was also realized that there was inadequate shielding of the metal traces on the chip; signals on different traces were coupling through the mostly undoped substrate.

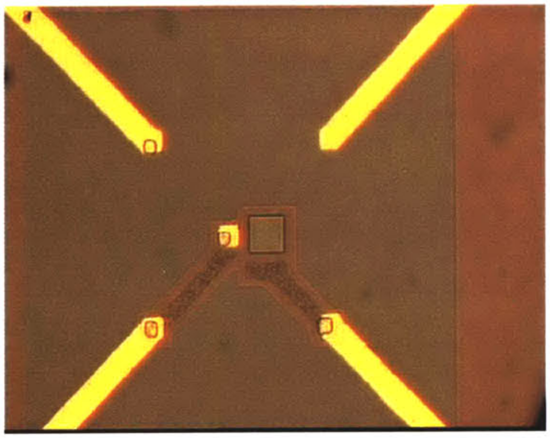

Fig. 3.2: Second-generation device, showing (clockwise from top left) substrate contact, unconnected trace, sensor trace, fluid bias trace. Sensor area is 80x80μm.

Fig. 3.3: Close-up of a second-generation device, Showing fluid reference electrode (left) and sensor. Sensor area is 50x50μm.

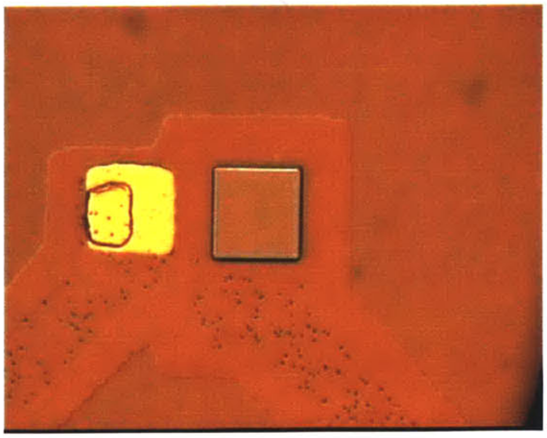

3.3 Process development

Several key issues dictate the design of the third generation field-effect sensor chips. First, the sensors should be as responsive as possible to changes in surface potential. As shown in section 2.1, the silicon depletion width decreases as the carrier concentration increases. Thus, the p-type sensor region must be as lightly doped as possible, in order to maximize the change in depletion capacitance resulting from changes in surface potential. A deep sensor implant maximizes the absolute capacitance range. Furthermore, an approximately uniform doping level in the sensor yields a predictable response to surface potential modulation.

Good electrical isolation is essential between the two sensor regions if useful differential signals are to be measured. Strong isolation between the fluid reference electrode and the sensors is also important, to ensure that any current measured by the sensors is passing through the electrolyte rather than simply leaking through the substrate. For these reasons, the sensor regions are implanted as oppositely doped p-type wells in an n-type substrate. The substrate is also supplemented with a heavy dose of phosphorus, creating an n+ top layer. Highly-doped p+ traces are used to connect the p-type sensors to the metal traces. These implants are necessary, as connecting to the sensors directly with metal would prohibit a microfluidics overlay. With this design, all signals are constrained to p-type silicon areas in an n-type substrate. As long as the voltage levels on the p-type traces are less than a diode drop above the substrate potential, there should be little leakage current.

It should be ensured that surface charge modulation at the sensors is the only figure being measured; changes within the rest of the microchannel should not be detected. For this purpose, the entire chip (with the exception of the active sensor regions) is passivated with a thick film of silicon-rich nitride. Nitride (Si_3N_4) was chosen to be field insulator for several reasons. First, it acts as a diffusion barrier for the implanted dopants, resulting flatter post-anneal implant profiles. Earlier generation devices used a thick, thermally diffused field oxide, which resulted in the loss of dopants near the silicon surface. Second, a nitride top layer is compatible with planned future developments such as integrated on-chip heaters.

The trace metal is gold, with a thin titanium adhesion layer. Gold was selected for its biocompatibility, resistance to degradation, and ease of deposition. The primary disadvantage of using gold is that the devices may not be sintered after metal deposition, as the gold would diffuse into the substrate. Omitting the sintering step results in a higher contact resistance than would ordinarily be seen with a standard process where aluminum is used for back end metallization. The use of gold also requires some special handling in the fab, so that non-gold process tools are not contaminated. Metallization is one of the final steps, however, so this is not of much concern.

The fluidic channels are fabricated out of (poly)dimethylsiloxane (PDMS). PDMS is a clear, flexible silicone elastomer in which shallow relief patterns (fluid channels) may readily be formed. The basic processing of PDMS is described in [7, 8], whereby SU-8 (a photosensitive material) is spun on a silicon wafer and patterned with a photomask. The unexposed SU-8 is developed away, leaving behind a negative image of the channels on the wafer. PDMS is then spin-coated or poured on the wafer, cured at a high temperature, and peeled off.

Due to inaccuracies with the EV1 contact mask aligner at the MTL Technology Research Laboratory, the silicon design is tolerant to alignment errors of up to ten microns in the x- and y- directions. Visual inspection after EV1 patterning in the past has shown alignment errors of up to five microns, particularly in the y- direction. While using the Nikon stepper at MTL Integrated Circuits Laboratory would have reduced alignment errors, fabricating a variety of die types would not have been possible.

3.4 SUPREM simulation

SUPREM process modeling software was used to determine ion implant and dopant annealing parameters. The device modeled by SUPREM used a simplified geometry in order to expedite the simulation time. This device had five distinct regions that are analogous to regions of the actual sensor chip: n+ implant, bare n-type substrate, p+ implant, p and p+ implants, and p implant. The full simulation code is listed in Appendix A.

The substrate resistivity was set to 20Ω-cm, at the low end of the 20-50Ω-cm range specified for the actual device wafers. High resistivity substrates were used so that the lightly-doped p-type sensor implants of 10^{15} cm^{-3} would still be an order of magnitude above the n-type substrate background concentration of 10^{14} cm^{-3}. 1-dimensional (vertical) dopant concentration profiles for each region were generated (Figs. 3.1 and 3.2). The simulation results indicate that a 240-minute inert anneal at 1050°C produces a nearly flat boron concentration profile in the sensor regions, with a junction depth of approximately one micron. The nitride field insulator serves as a diffusion barrier for the implanted species, keeping them in the silicon. Both the p+ conductive traces and the n+ substrate implant were adjusted to reach maximum concentrations of approximately 10^{19} cm^{-3} near the silicon surface. A 2-dimensional plot indicated that lateral diffusion is less than 2μm at all boundaries.

SUPREM was also used to determine dry SiO_2 growth times for the 30nm implant oxide and the 50nm pad oxide beneath the nitride. Section 4.2 compare the predicted film thickness values and post-anneal sensor dopant profile to those measured after fabrication.

Implant region	Species	Dose	Energy
p+ (traces)	Boron	$2 \cdot 10^{15}$ cm^{-2}	150keV
P (sensors)	Boron	$2 \cdot 10^{11}$ cm^{-2}	200keV
n+ (substrate)	Phosphorus	10^{15} cm^{-2}	200keV

Table 3.1: Parameters for three implanted regions.

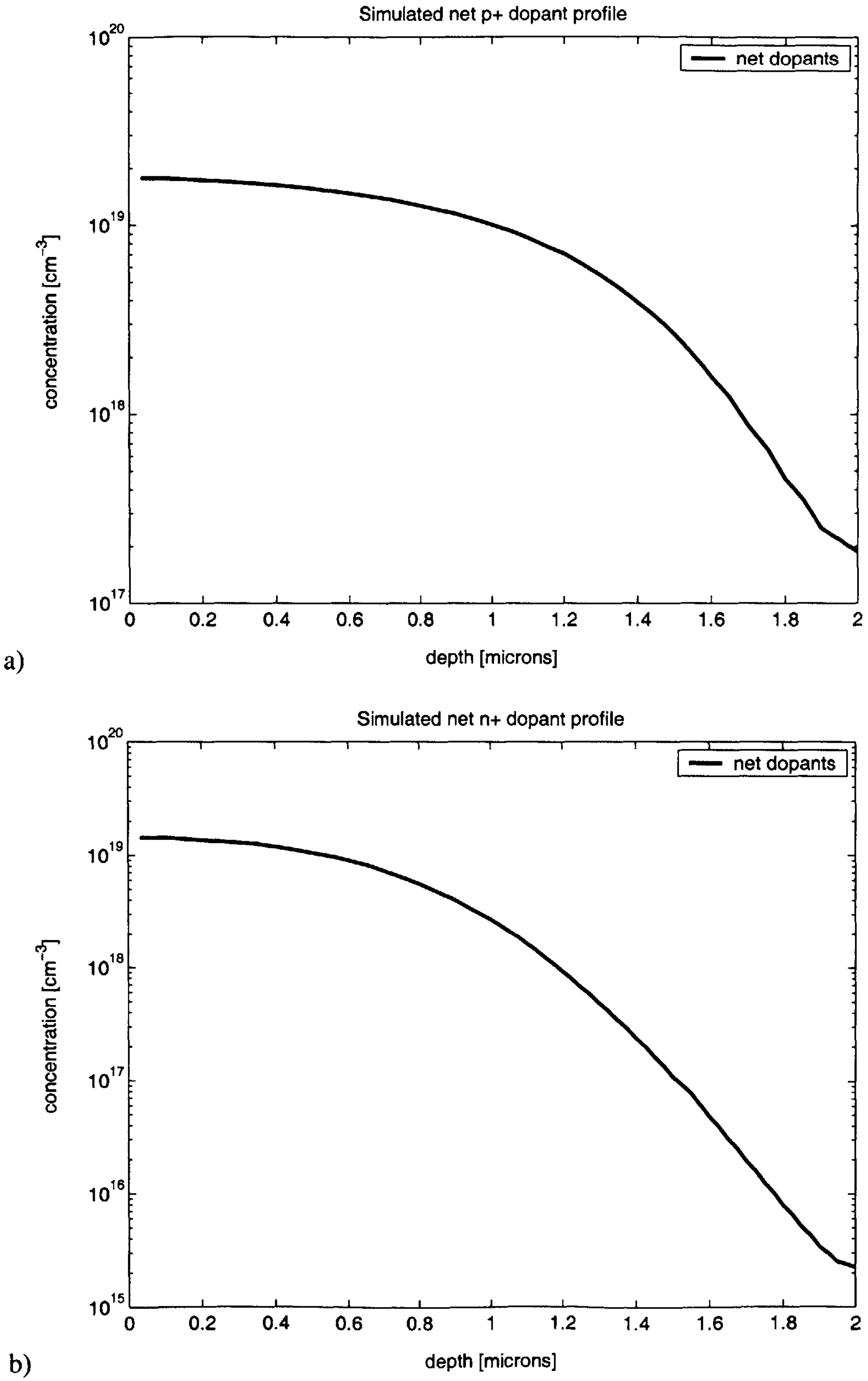

Fig 3.4: Simulated post-anneal dopant profiles in p+ conductive traces (a) and n+ implanted substrate (bottom).

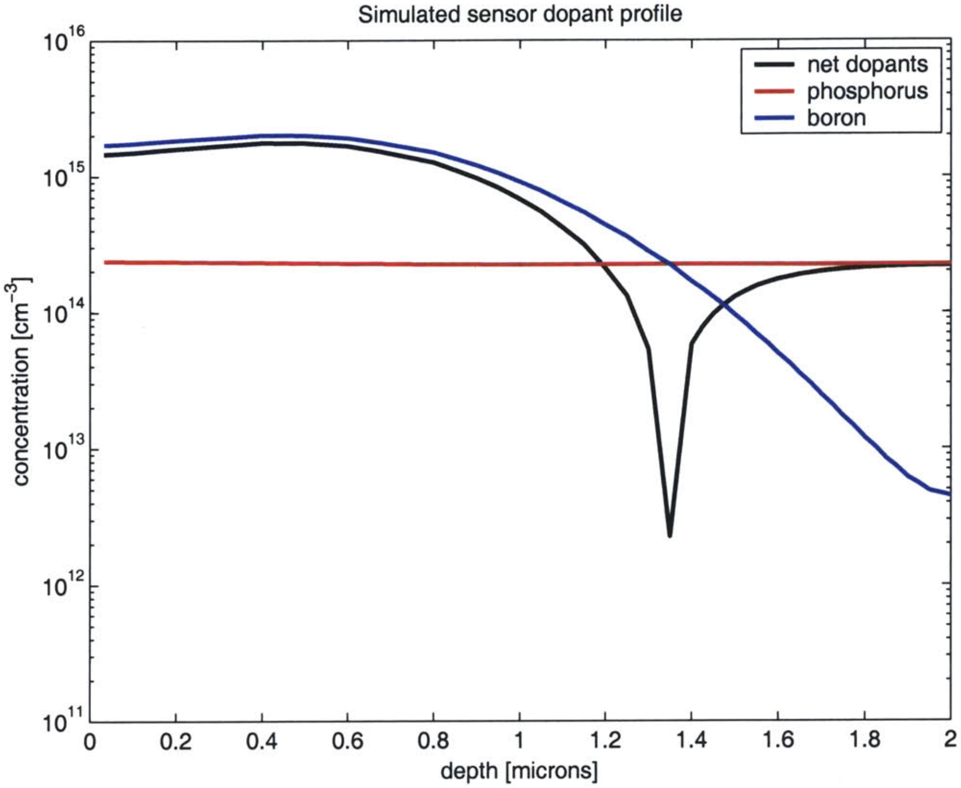

Fig 3.5: Simulated post-anneal dopant profile in inverted p-type sensor region.

3.5 Geometry and device types

The basic two-sensor chip geometry shown in Fig. 3.6 has two sensors and a shared reference electrode in a 100μm-wide microfluidic channel. The center-to-center distance between the two sensors is 800μm. Assuming a channel height of 60μm, width of 100μm, and fluid plug length of approximately 1mm (in order to span both sensors), the theoretical minimum fluid volume is 100μm x 60μm x 1000μm = 6nL, a vast improvement over previous designs which use bulky external fluid cells and fluid volumes on the order of microliters.

Metal trace routing is designed to enable maximum flexibility with the layout of overlayed PDMS channels. The only restrictions on the placement of PDMS channels are that the 1mm-diameter entry points for PE tubing cannot be closer than approximately 2mm to one another (to prevent the PDMS from cracking), and approximately 1.5mm must be left clear at the edges of the chip to leave room for wirebonds.

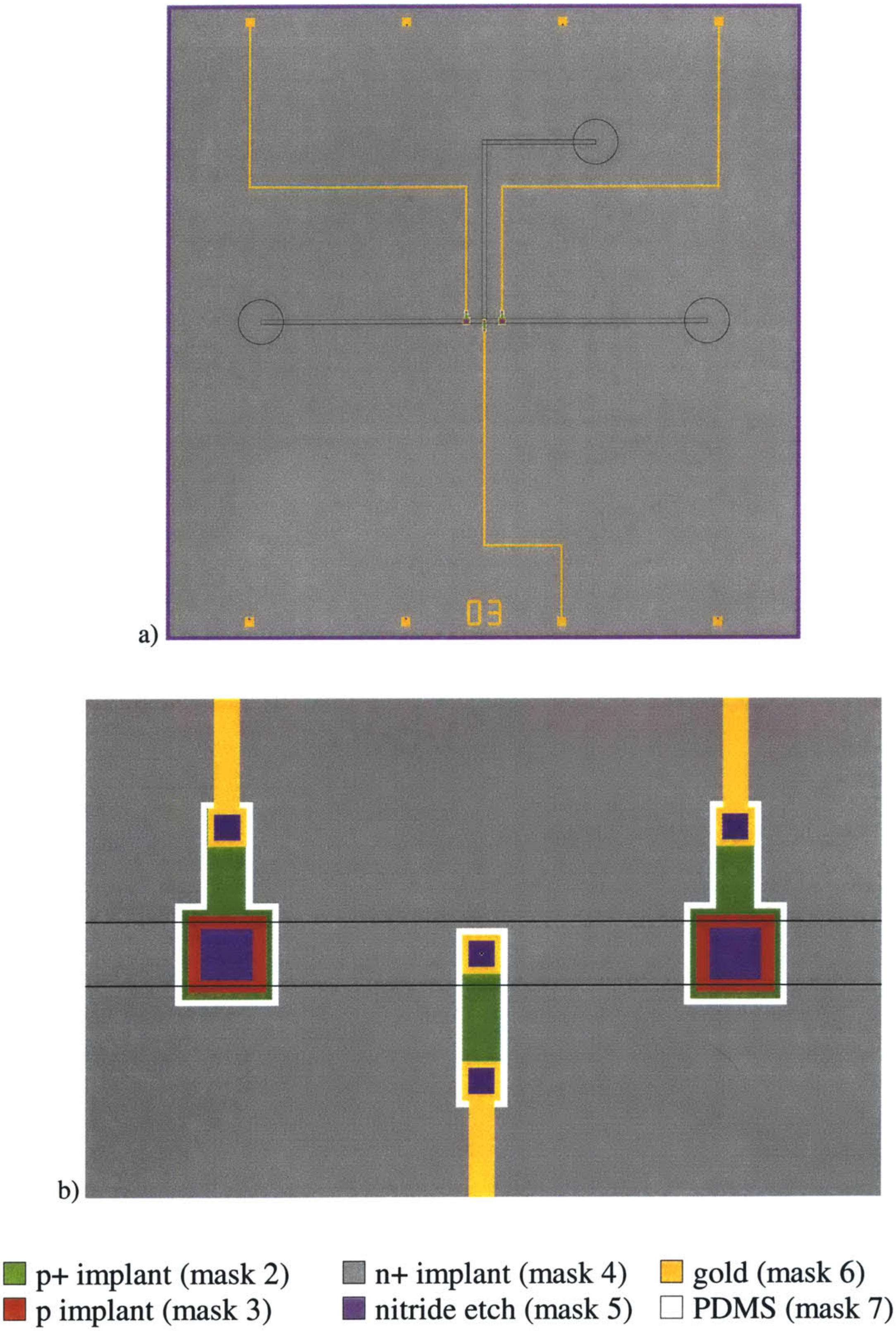

Fig. 3.6: (a) Die 3 layout. Edge dimension = 14mm.
(b) Close-up of die 3 sensor area. Sensor dimension = 80x80μm.

To simplify the initial device testing, a single 10mm-long straight channel (Fig. 3.6b) was used to ease the delivery of fluids to the sensors. Future work may include the design of more complex fluidic structures that fit on the 14x14mm footprint of the silicon die. The fluid volumes used during initial testing were also much larger than the theoretical minimum detectable volume of 6nL.

Eleven different device types were designed, and included in the maskset in different quantities. The variety of device geometries enables different microfluidic overlays to be designed, and different sensor sizes and configurations to be tested. In addition, some of the devices listed (8, 9, and 10) were designed specifically for testing purposes only. The various devices are summarized in the following table:

Device type	**Number of sensors**	**Sensor edge dimension**	**Bias electrode?**	**Sensor to electrode distance**	**Notes**	**Quantity on wafer**
1	2	20μm	Yes	400μm		4
2	2	50μm	Yes	400μm		16
3	2	80μm	Yes	400μm		8
4	2	50μm	Yes	400μm		4
5	2	50μm	Yes	400μm		4
6	2	50μm	No	N/A		4
7	1	50μm	Yes	200μm		2
8	2	50μm	No	N/A	Metal-gate test device	2
9	1	50μm	No	N/A	Metal-gate test device	2
10	0	N/A	No	N/A	Metal traces only	2
11	2	50μm	Yes	200μm		2

Table 3.2: Field-effect sensor chip die types. Fifty 14x14mm dies fit on each 6” device wafers.

3.6 Test structures and mask design

In addition to the 50 device dies on the wafer, two dies containing test structures and alignment marks were also included in the maskset. Some test structures, such as sets of horizontal and vertical lines and spaces, were used during fabrication to evaluate exposure and development parameters. Other test features, such as Van Der Pauw structures, 32-square resistors, and metal capacitors, were intended for testing after fabrication to determine dielectric thicknesses and sheet resistivities of implanted layers. The metal pads connecting to the electrical test features were specifically layed out to be compatible with a probe card in use at MTL.

Mask files were produced with Macromedia Freehand 9.0. While not intended for silicon mask design, Freehand is commonly used at M.I.T. for preparing microfluidics transparency masks. As the design of the sensor chips originally started with microfluidics, it was natural to use Freehand for the entire project. Unfortunately, Freehand does not have the full feature set expected of a conventional mask-making package such as Cadence. For example, there is no cell management; if a small correction had to be made to a particular die type after the wafer layout was completed, each die had to be corrected individually. In addition, the output files had to be converted several times before they could be used for chrome photomask production; the individual layers were first exported as Encapsulated Postscript (.eps) files, then converted to Autocad (.dxf), then to GDSII. Chrome masks were produced at Advance Reproductions, North Andover, MA, using optical photogeneration with a critical dimension of 10μm.

4. FABRICATION AND PACKAGING

4.1 Field-effect sensor chip fabrication

With the exception of three ion implantation steps, fabrication of the integrated field-effect sensors and microfluidics was carried out at the MIT Microsystems Technology Laboratories (MTL). The starting materials were 6-inch n-type silicon wafers doped with phosphorus, sheet resistivity 20-50Ω-cm. The substrates were purchased from WaferNet, San Jose, CA. A lot of ten wafers was started, with a single wafer (designated as #5) completing the entire process.

The first processing step was to etch global alignment marks in the wafers. As ion implants cannot readily be seen optically, visible global alignment marks are necessary for the registration of the implant masks. The alignment marks were etched with a LAM490 plasma etcher. The "black silicon" recipe that was used is high in chlorine, which rapidly attacks silicon and turns the etched pattern black. Next, the photoresist was ashed and the wafers were cleaned with a Piranha (3:1 H_2SO_4 : H_2O_2) dip, then in an RCA bath. 30nm of dry thermal SiO_2 was grown in 60 minutes at 950°C (Fig. 4.1a). This thin oxide film served to protect the silicon from surface sputtering during subsequent ion implantation.

Photoresist was spin-coated, and the wafers were patterned with the p+ implant mask. The wafers were sent to Implant Sciences Corporation, Wakefield, MA, for the p+ (boron) implant (Fig. 4.1b). Upon returning to the fab, the photoresist was stripped and the wafers cleaned with a double Piranha dip. Since the p+ implant dose was relatively large, the baked resist stripped off in flakes rather than dissolving in Piranha. After cleaning, the wafers were again spin-coated with resist, patterned with the p implant mask, and sent out for implant (Fig. 4.1c). Upon return, they were again dipped twice in Piranha, re-coated with resist and patterned with the n+ implant mask.

After the n+ (phosphorus) implant (Fig. 4.1d), the resist was removed and the wafers were cleaned with a double Piranha dip. The thin oxide layer was stripped with a one minute Buffered Oxide Etch (BOE) dip (Fig. 4.1e). Next, a fresh 50nm layer of dry thermal SiO_2 was grown in 60 minutes at 1000°C (Fig. 4.1f). A 1μm thick layer of low-stress silicon-rich nitride (Si_3N_4) was then deposited on top of the pad oxide in a vertical thermal reactor (VTR) immediately after the oxide growth (Fig. 4.1g). The nitride was deposited at a sufficiently low temperature to avoid too much dopant diffusion within the silicon. After nitride deposition, the wafers were annealed for four hours at 1050°C to flatten the dopant profile in the sensor regions (Fig. 4.1h). This step also served to drive-in the implanted species, activating them by incorporating them into the silicon lattice.

After annealing, photoresist was spin-coated, and the wafers were patterned with the nitride etch mask. The pattern on this mask defines the metal contact holes and the active sensor regions. The contacts were plasma etched (Fig. 4.1i) with an Applied Materials AME5000, using a CF_4 etch chemistry. An effort was made at first to preserve at least some of the 50nm of SiO_2 below the nitride, after which the oxide could be wet etched, preserving the integrity of silicon surface. Due to time constraints, however, it was decided to proceed with a single etch that went all the way through to the silicon.

After the contact holes were etched, the resist was ashed, and image reversal photoresist was spin-coated. Image reversal photoresist yields negatively sloped sidewalls, enhancing the edges of metal traces when a lift-off process is used. The wafers were patterned with the metal interconnect mask, and were ashed for five minutes to remove any photoresist residue in the patterned areas that was not fully developed. The wafers were then dipped in BOE for one minute to strip any native SiO_2 which may have formed at the contacts. 20nm of titanium and 1μm gold was deposited with an electron-beam evaporator.

After metal deposition, the wafers were soaked in acetone overnight to lift off the metal that was deposited on top of the resist, leaving behind the metal deposited in the clear areas (Fig. 4.1j). An ultrasonic bath may be used to expedite the lift-off process, however this may result in rough trace edges or complete removal of all metal from the silicon surface if adhesion is poor. For this process, it was decided soak the wafers overnight, thus avoiding any potential adhesion issues. After the overnight soak, the wafers were gently sprayed with methanol and isopropanol to peel back the gold, after which they were rinsed and spin-dried. A final layer of photoresist was spin-coated to protect the frontside of the wafers from dust while dicing.

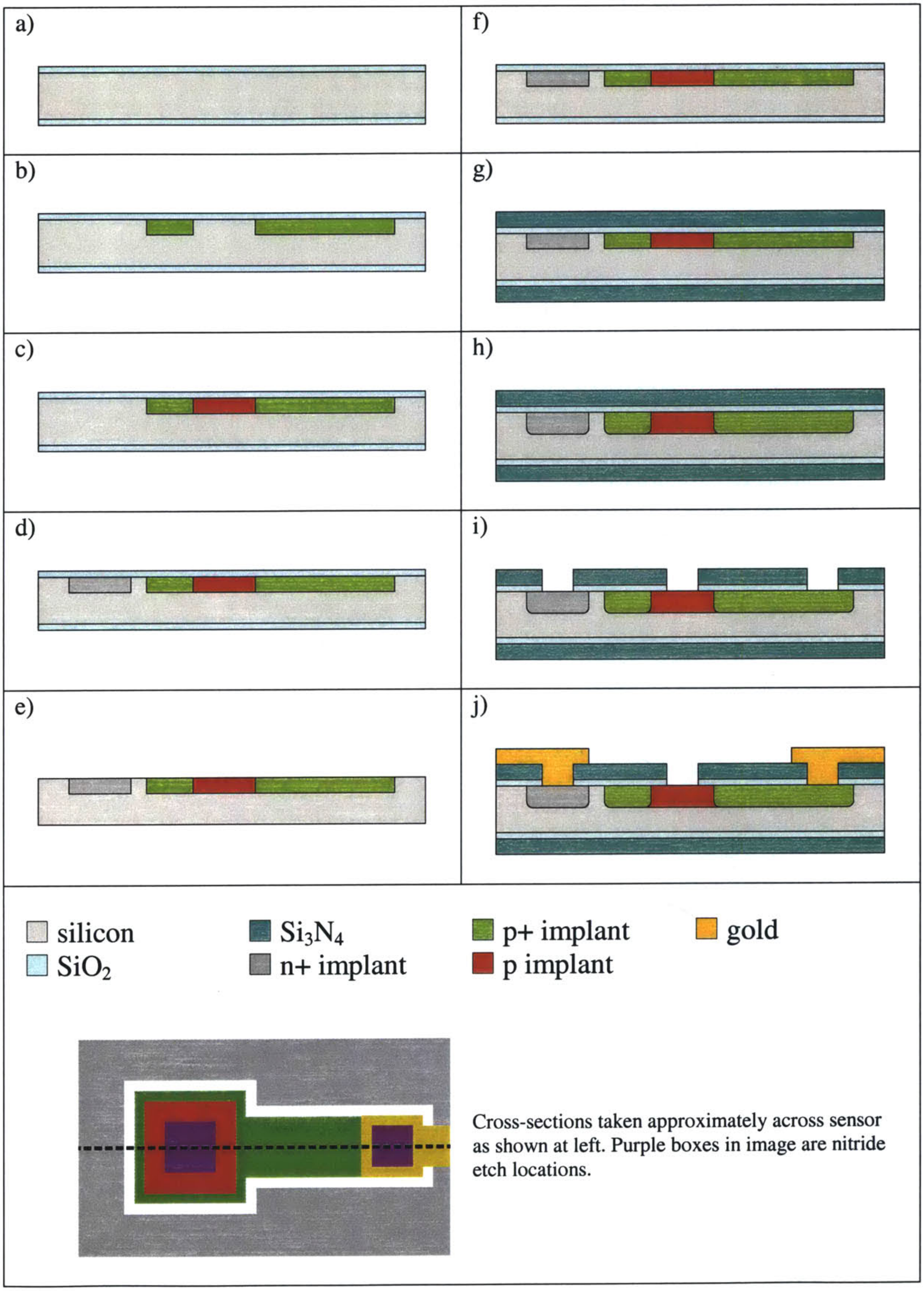

Cross-sections taken approximately across sensor as shown at left. Purple boxes in image are nitride etch locations.

Fig. 4.1: Cross-sections of field-effect sensor chip fabrication steps.

4.2 Sensor chip fabrication results

One wafer (#EIS2-5) completed the entire microfabrication process, while the other wafers were intentionally left at various intermediate stages. The figure below shows a 10x optical micrograph of a sensor and reference electrode on a type 2 (dual 50x50μm sensor) die:

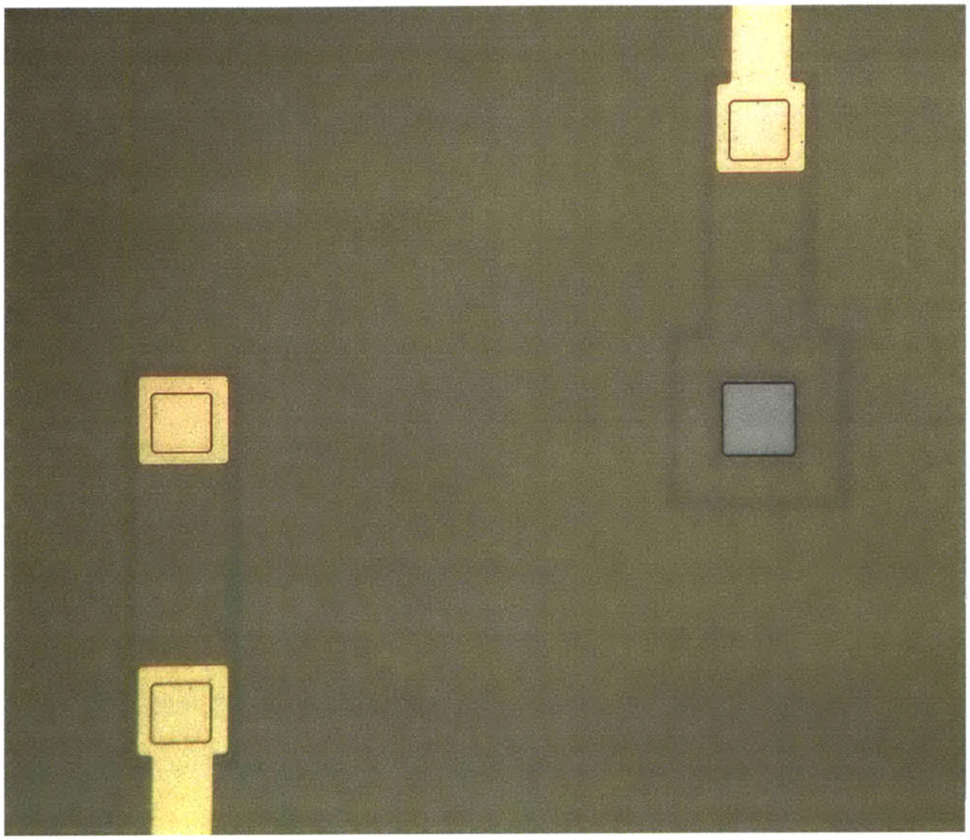

Fig. 4.2: 10x optical micrograph of bias electrode (left) and 50x50μm sensor. An overlayed microfluidic channel would be oriented horizontally to enclose the electrode and the sensor. (p+ dose on this device is higher than on others, making p+ traces visible)

Inspection of the alignment marks indicated that all of the layers were registered to within five microns of each other, well within the ten micron tolerance. Figure 4.3 shows nitride etch and gold alignment crosses as compared to the global alignment boxes. The crosshairs are 10μm wide, while the box spaces are 20μm wide. The yield on wafer #EIS2-5 appeared to be 100%.

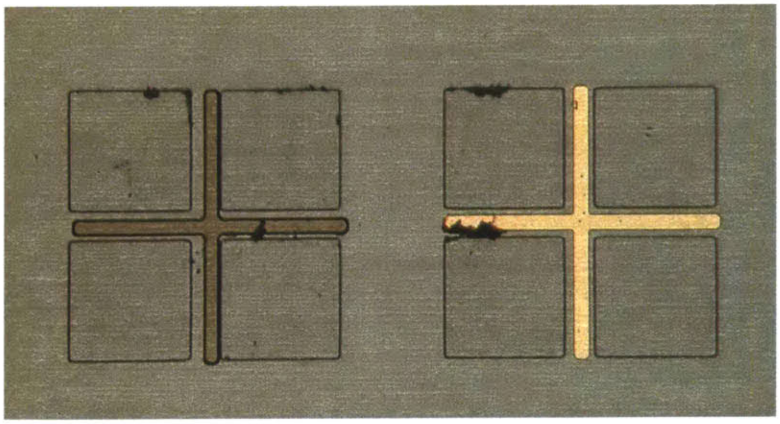

Fig. 4.3: Nitride etch (left) and gold crosses, aligned to global alignment boxes. Crosshair width = 10μm.

The metal liftoff was very successful; gold adhesion to the substrate was strong, and the edge definition was much better than the results obtained with transparency masks and standard positive photoresist. Gold in certain small interior spaces (for example, some lithography test patterns) did not lift off, but this was not entirely unexpected.

A lightly-doped p monitor wafer was sent to Solecon Laboratories, Reno, NV, for spreading resistance analysis (SRA) to determine the vertical implant profile at the sensor locations. In an SRA test, a sample is first "beveled" at a shallow angle, then a miniature four-point probe takes incremental resistivity measurements down the bevel. A profilometer measures the exact bevel angle to accurately map the resistivity data to sample depth.

The SRA results for the monitor wafer confirm a light Boron implant in an n-type substrate. The substrate dopant concentration is 10^{14} cm^{-3}, corresponding to a sheet resistivity of 40Ω–cm [16]. The peak boron concentration of $1.26 \cdot 10^{15}$ cm^{-3} occurs at a depth of 110nm, and there is an expected drop in dopant concentration at the surface due to diffusion into the oxide layer. The most surprising result is the shallow junction depth of 600nm, as SUPREM simulation predicted a post-anneal junction depth of approximately 1μm. Possible explanations for this discrepancy are that the implant energy was less than 200keV, or that there was considerably more boron diffusion through the nitride than was predicted.

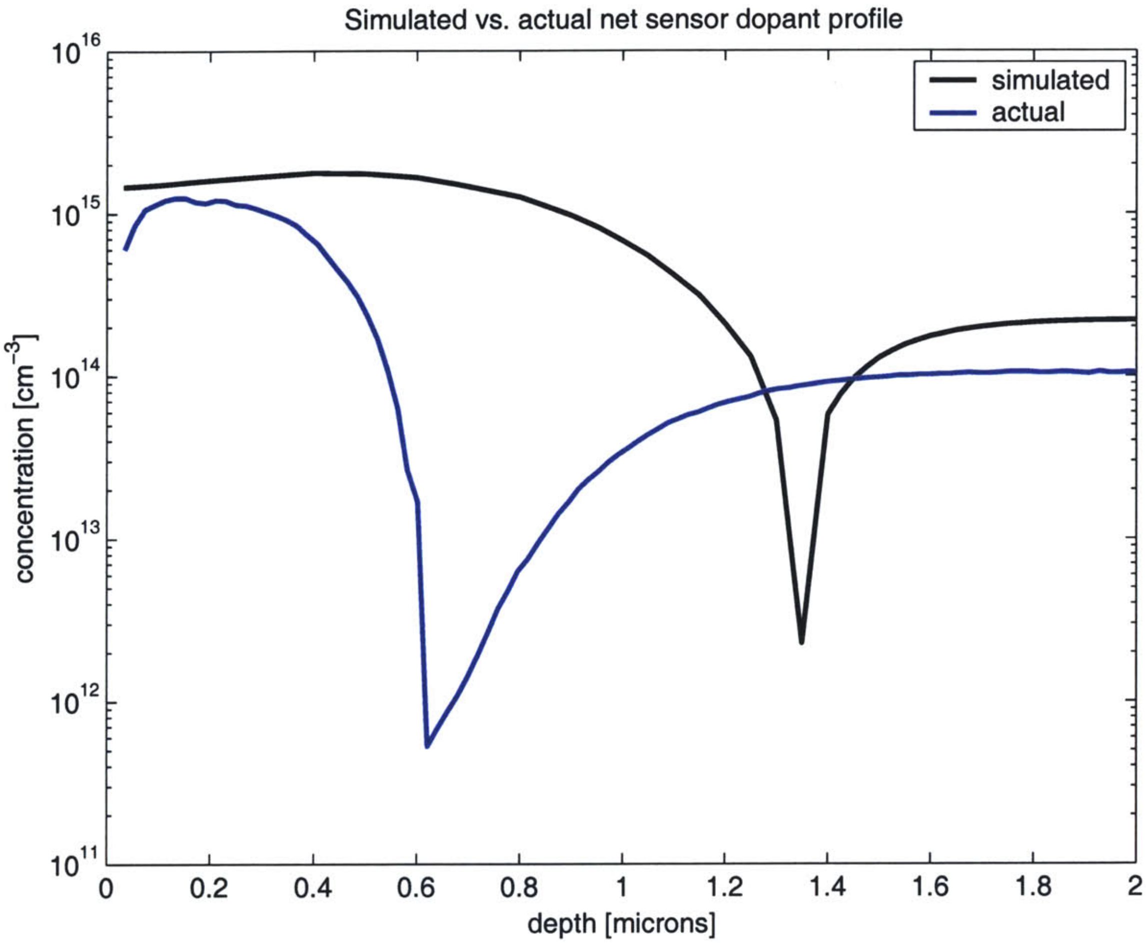

Fig. 4.4: Comparison of simulated and actual sensor dopant profiles.

Dopant profiles aside, SUPREM was right on target with its film thickness predictions. Table 4.1 compares the thickness of SiO_2 layers as predicted by SUPREM, and as measured with a KLA-Tencor UV1280 system.

Diffusion step	**Time**	**Temperature**	**SUPREM thickness**	**Measured thickness**
Implant oxide	60min	950°C	30nm	30nm
Pad oxide	60min	1000°C	49nm	53nm

Table 4.1: Predicted vs. actual SiO_2 film thicknesses.

4.3 PDMS microfluidics fabrication

The fabrication of PDMS microfluidics consists primarily of patterning a "master" mold wafer, onto which PDMS is cast or spin-coated. Microfluidics fabrication is relatively straightforward, and the process has evolved to the point where it is extremely reliable and only a few hours of work are necessary to produce channels. To create the microfluidics for this project, a 4-inch silicon wafer was first baked for twenty minutes at 100°C to dehydrate the surface, thus promoting photoresist adhesion. Next, it was spin-coated with SU-8 (Microchem SU-8 50), a thick negative photoresist, and soft baked for 10 minutes at 100°C.

The wafer was exposed to a dark-field transparency photomask placed emulsion-side down, and held in place with a glass sheet. A 1:40 exposure time yielded excellent results. Some early master wafers had "T-topped" PDMS patterns (Fig. 4.5), where the channel traces were wider on top than on the bottom. This problem arose due to overexposure, and poorly filtering of the UV exposure lamp.

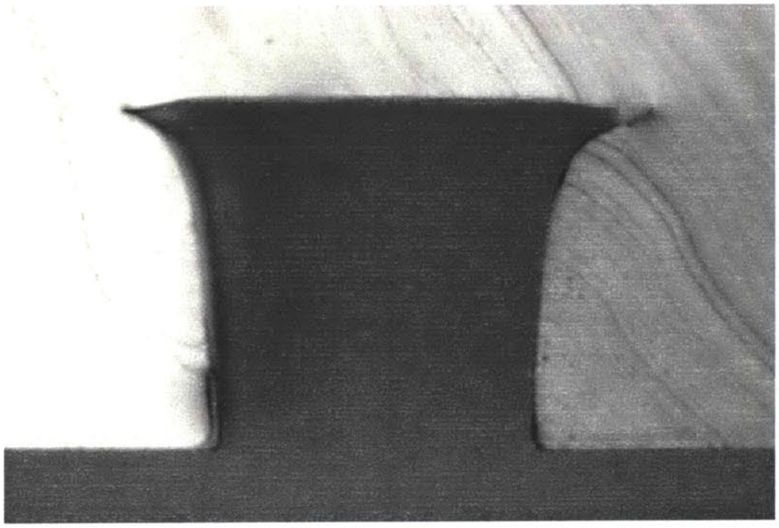

Fig. 4.5: "T-topped" SU-8 profile, resulting from overexposure and poorly filtered exposure lamp.

After exposure, the wafer was again baked for five minutes at 100°C. It was then developed for approximately five minutes in PGMEA-based SU-8 developer. Residue left behind by the developer was removed by rinsing in acetone, after which the wafer was rinsed in water and dried with an air gun. The next step was for the wafer to be silanized, a step with coats the wafer with a non-stick Teflon-like monolayer so that cured PDMS will not stick to the surface. The wafer was placed in a chamber with several drops of (tridecafluoro-1,1,2,2-tetrahyrooctyl)-1-trichlorosilane and held under vacuum for two hours.

Next, the two prepolymer components of poly(dimethylsiloxane) (Dow-Corning Sylgard 184) were mixed together in a 10:1 ratio of part A to part B. 10:1 is the standard mixing ratio, but this may be modified to yield harder or softer PDMS. The mold wafer was placed in a 6"-diameter plastic petri dish, and the mixed PDMS polymer was poured over the wafer. The PDMS was de-gassed by holding it under vacuum for approximately 30 minutes. After de-gassing, the PDMS was cured at 80°C for 30 minutes. Over-curing hardens the PDMS, making it difficult to punch insertion holes for the fluidics. Under-curing leaves the PDMS sticky and prone to cracking when tubes are inserted. After curing, the PDMS was peeled from the mold wafer and diced with a razor blade.

4.4 Packaging

After the silicon device wafers are diced, individual dies are cleaned with acetone, methanol, and isopropanol, then rinsed with DI water and blown dry with an air gun. Some dies may be further prepared by dipping them into Buffered Oxide Etchant (7:1 H_2O : HF) for 30 seconds, rinsing in DI water for 30 seconds, dipping in Piranha solution (1:1 H_2SO_4 : H_2O_2) for 30 seconds, rinsing again in DI water, and drying them with an air gun. This procedure is based on the device cleaning done in [4, 6]. The BOE strips the native SiO_2 on the sensor surfaces at approximately 700Å/sec (easily removing the 20-30Å of native oxide during the 30-second etch), and the Piranha solution regrows a chemical oxide of several nanometers.

Separate from the silicon die preparation, PDMS dies are punched with a modified syringe needle to create insertion holes for polyethylene (PE) tubing. The needle's syringe tip was ground off, and the outer sidewalls were tapered. An 18-gauge needle is used to punch the holes, into which PE tubing with outer diameter .043" is later inserted for fluid delivery. Next, the PDMS dies were covered with VWR lab tape to remove surface dust. Solvents are never used to clean the PDMS dies prior to bonding, as they may be absorbed by the PDMS, causing severe swelling that could affect the alignment process. It should be noted that 10:1 A:B PDMS contracts slightly while curing. While this contraction was not accounted for when designing early test devices, it will be essential to when designing more complex PDMS devices that must precisely mate with patterns on the silicon.

It has been shown that treating PDMS in an oxygen plasma causes it to bond permanently with certain other surfaces when similarly treated [7, 8]. A strong bond is essential for pumping fluids on-chip at high pressures. The silicon and PDMS dies were treated with a Harrick PDC-32G plasma cleaner using air as the inflow gas, adjusting the flow rate so that the plasma was bright pink in color. It was determined experimentally that a 30-second treatment at high power resulted in a strong bond between PDMS and Si_3N_4 surface of the sensor die. The surface activation of the PDMS lasts for only about five minutes, so the pieces had to be bonded very quickly after plasma cleaning to ensure a strong seal; in the lab, pieces were aligned and bonded within two to three minutes of exiting the plasma.

After plasma treatment, the two separate components were loaded into a mask aligner using custom laser-cut acrylic adapters. One adapter fits where a photo mask would ordinarily be mounted, and holds the PDMS die. The other adapter is mounted on the waferchuck and holds the sensor die. The sensor die and PDMS are brought into close proximity and aligned by hand using the mask aligner's x-, y-, and θ- micrometers. The two components are brought into contact by slowly raising the aligner's contact lever. An alignment precision of 5μm between the silicon and the PDMS was regularly achieved with this technique. After waiting several minutes for the bonding to occur, the integrated module is removed from the aligner and excess PDMS is cut with a razor.

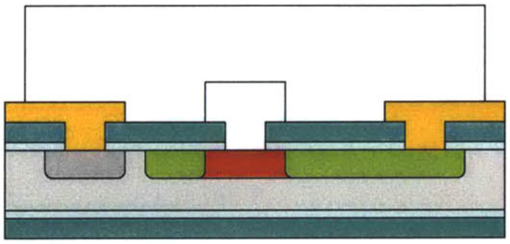

Fig. 4.6: Cross-sectional schematic diagram of integrated silicon die and PDMS.

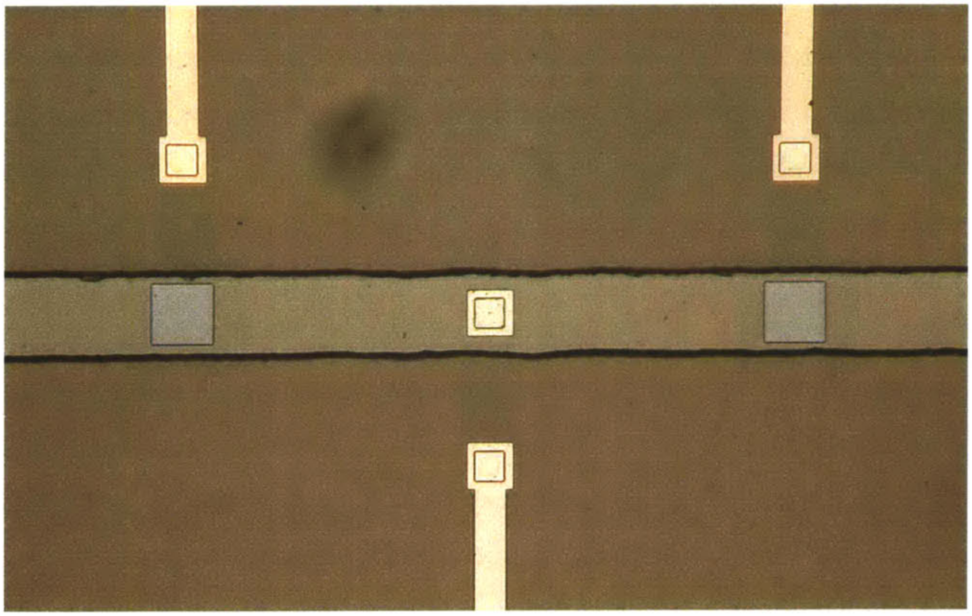

Fig. 4.7: 10x optical micrograph of sensor chip with aligned 100μm microfluidic channel.

Next, the module was epoxied to a custom printed circuit board (PCB) package. Aluminum wirebonds (wedge-wedge) were used to make connections between the chip and the PCB. As wirebonds will not stick to the usually tin-lead solder coated traces of a PCB, the boards were manufactured with gold-plated traces. In testing, the wirebonds adhered strongly to the gold surface. An RTV silicone coating may be used to protect the delicate wirebonds, however this is not necessary if the devices are handled delicately during testing. 2mm header pins on the bottom side of the board enable the chip module to be plugged into a socket for testing. Finally, polyethylene tubing was inserted into the holes previously punched in the PDMS.

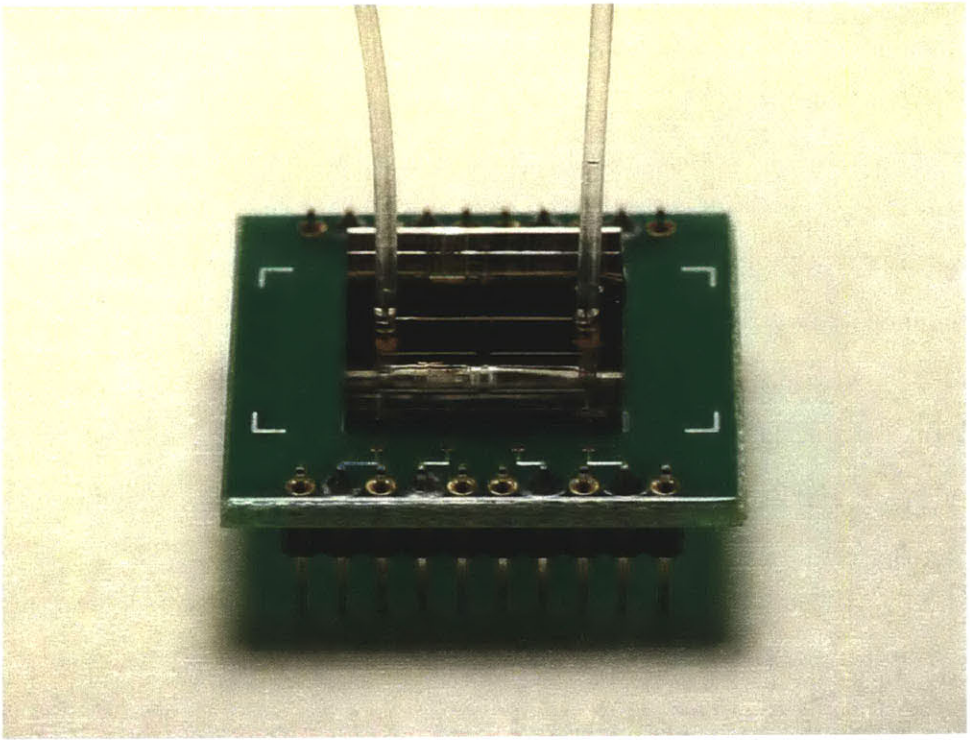

Fig. 4.8: A packaged device, with polyethylene tubing inserted.
The package edge dimension is one inch,

5. TESTING AND RESULTS

5.1 Laboratory test setup

The packaged device modules plug into a printed-circuit breakout board, which is mounted inside an aluminum enclosure. The enclosure is grounded, and shields the devices electrically and optically. In particular, the devices are very sensitive to light, as light striking the sensors and substrates of the chip results in the optical generation and recombination of carriers in the silicon, causing the devices to act as photodetectors. SMA bulkhead jacks are used to interface to the chip leads. A microscope for monitoring the delivery of fluids is mounted above the setup, although the lid to the enclosure must be closed during data collection. The polyethylene tubing that delivers fluids to the chip exits the enclosure through a hole in the lid. A small amount of light leaks in through this hole, so the tubing is kept inside the enclosure whenever possible, and the enclosure in wrapped in aluminum foil.

An external fluid switching mechanism using flexible tubing and solenoid pinch valves (Bio-Chem, Inc., P/N 100P2NC12-018) has been set up. A custom circuit board using ULN2003 Darlington sink arrays was built to allow control of the 12V solenoid valves with 5V logic signals, thus allowing Labview software to control the fluid switching.

With the external switching mechanism, the electrolyte inside the microfluidic channel may be replaced without having to inject new fluids by hand. Manually switching the fluids results in capacitive coupling to the sensors through the conductive electrolyte, and subsequent measurement drift. The valves also enable the fluids to be replaced with no air gaps. Air in the microfluidic channel results in a temporary signal loss when no fluid is in contact with the sensors or reference electrode. When the signal returns, there is a spike in the output and then a relaxation period (see section 5.3.3 for a plot showing this behavior).

Air pressure is used to push fluids through the sensor chip. In the test setup, fluid is first pulled through an 8-inch long segment of rubber tubing with a syringe. Next, the back of the tubing is opened to a 1-2psi stream of air. When the mechanical pinch valves are opened, the back pressure on the fluid moves it through the microfluidic channel and onto the sensor. Using this method, the fluid contacting the sensors may be replaced in less than ten seconds.

Future device development will include the integration of PDMS air-controlled valves, enabling rapid on-chip fluid switching. Such valves have already been designed and fabricated, and are discussed in Appendix C. This integration step will reduce the amount of dead volume in the system, minimizing the amount of fluid necessary to make a measurement. It will also enable the selective functionalization of individual sensor surfaces, a capability that is essential for differential measurements.

A rack of electronics test equipment is used to take measurements. The substrate bias is set using a DC power supply (Agilent E3630A). The fluid bias electrode is driven with a function generator (Stanford Research Systems DS345), which is controlled by Labview via GPIB interface. Each sensor's tiny output current is boosted by a current amplifier (Keithley 428), with gain generally set to 10^6 or 10^7. The current amplifiers are connected to lock-in amplifiers (SRS SR850), which are locked to the AC drive frequency. The lock-in amplifiers output the root-mean-square amplitude of the input signal (at the drive frequency) to a National Instruments analog data collection system, which connects to Labview. The collected data is imported into MATLAB for analysis and plotting.

To maximize the sensitivity of the measurement system to small changes in surface potential, the sensors are biased at the steepest part of their depletion curves, and offsets are applied at the lock-in amplifiers to null the output signals. An internal "expansion" setting is increased to expand the output swing in response to small deviations around the operating point.

5.2 Dry testing

In order to fully characterize the devices, many dry electrical tests were performed before any testing with electrolytes. First, to verify the accuracy of the electronics setup and subsequent MATLAB processing, a 22pF ceramic capacitor was plugged into the test socket. The capacitor was driven with a 100mV$_{pp}$ signal at 8kHz (the same drive amplitude and frequency used for later measurements), and the AC current was measured for ten seconds. The collected data was averaged, and the capacitance was determined to be 21.77pF, well within the 5% tolerance of the capacitor value. The same test was performed with a 68pF ceramic capacitor, and capacitance was measured to be approximately 66.10pF, again well within the 5% tolerance.

Next, a type three device (with five substrate contacts; see Fig. 3.6a) was plugged into the test board, and voltage measurements were taken at each contact point. As indicated in table 5.1, when substrate contact 4 was biased to 2.0000V, the voltage drop at every other contact point was 2.1mV or less, indicating that the resistivity of the substrate is low, and that it is an effective ground plane.

Contact #	Measured voltage	Voltage drop
1	1.9979V	2.1mV
2	1.9980V	2mV
4	2.0000V	0mV
6	1.9983V	1.7mV
7	1.9980V	2mV

Table 5.1: Voltage drops at substrate contacts, indicating low sheet resistivity.

Device type ten was used to determine capacitive coupling between metal traces. As seen in chapter 3, device type ten consists only of metal traces and an implanted substrate, and there is no reference electrode or sensors. Two pathways exist for capacitive coupling between traces: through the air, and through the substrate. First, measurements were taken with an ungrounded, floating substrate. Capacitive coupling between the two sensor traces was measured to be 2.04pF, and coupling between the reference electrode trace and a sensor trace was 1.53pF. The substrate was then grounded, and the same measurements were repeated. Coupling between the two sensor traces decreased to .1336pF, and coupling between the reference electrode trace and a sensor trace decreased to .0933pF. These results indicate a reduction in capacitive coupling between metal traces by a factor of approximately fifteen when the substrate is grounded (or biased at a constant voltage). Thus, when the substrate is grounded or DC biased, it is essentially eliminated as a pathway for coupling between metal traces. The results of this test are summarized in table 5.2.

Substrate connection	**Sensor-sensor coupling**	**Reference electrode – sensor coupling**
Floating	2.04pF	1.53pF
Grounded	.1336pF	.0933pF
(reduction factor)	15x	16x

Table 5.2: Capacitive coupling between metal traces, with floating and grounded substrate.

Simple diode tests were performed with a type three device, whereby a voltage sine wave was applied to a p-type sensor or reference electrode trace, and the output signal was measured at the n-type substrate. This testing configuration essentially forms a pn diode. The theoretical diode drop between a p-type sensor and the n-type substrate is:

$$\phi_B = \phi_n - \phi_p = V_{th} \ln\left(\frac{10^{14}}{10^{10}}\right) + V_{th} \ln\left(\frac{10^{15}}{10^{10}}\right) = 540\,\text{mV}$$

Figure 5.1 shows a 100Hz signal applied to a sensor, (blue trace) and the corresponding output on the substrate (red trace). The diode drop is seen to be approximately 450mV. One possible reason for smaller than expected diode drop is that the shallow slope of the dopant profile in the sensor region (see Fig. 4.4) effectively lowers the carrier concentration N_a near the junction. The reason for using such a low frequency (100Hz) for testing is that the large capacitive load of the substrate caused distortion at higher frequencies. While the results of the diode test were not quite as predicted, it succeeded in its purpose to simply to verify the presence of the activated p-type implant in the n-type substrate.

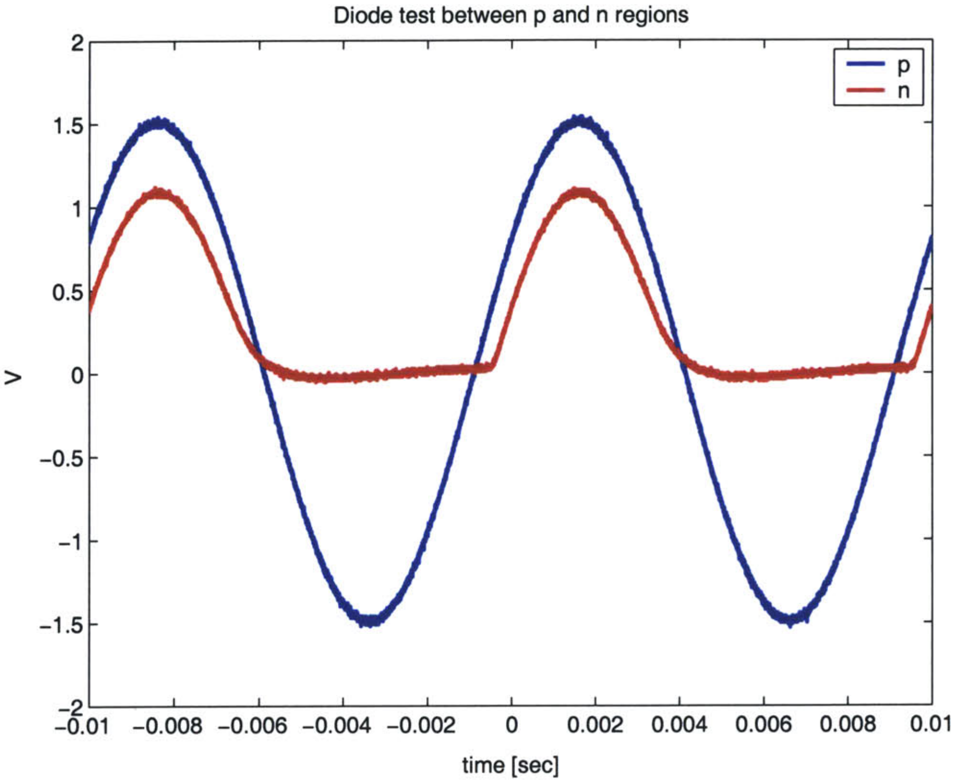

Fig. 5.1: Diode behavior between p-type sensor and n-type substrate.

Current leakage through the substrate, from the integrated reference electrode to the sensors, was measured. A 100mV_{pp}, 8kHz sine wave was applied to the reference electrode, and the AC current leakage into the sensors was measured. For this test, the substrate was first floated, then grounded, then biased to 2V. The results indicate a 9-fold reduction in the leakage current when the substrate is grounded or DC biased, once again demonstrating the importance of the implanted n+ substrate for good isolation between different regions of the chip.

Substrate connection	**Current leakage from ref. electrode to sensors**
Floating	90.5nA (rms)
Grounded	10.3nA (rms)
2V	10.3nA (rms)

Table 5.3: Current leakage between reference electrode and sensors.

5.3 Wet testing

In order to test the devices with an electrolyte, .01M phosphate buffered saline (PBS) was made by dissolving a tablet (Sigma P-4417) in 200mL Nanopure water. The solution was pulled with a vacuum pump through a cellulose acetate filter (Corning 430626) to separate out particles larger than .22um, which could potentially build up and clog the microfluidic channel. PBS was then manually injected into the sensor with a 50μL syringe, and capacitance-voltage curves, sensitivity figures, and pH response were measured.

5.3.1 Capacitance-voltage (CV) curves

Upon injection of PBS and the application of a 100mV$_{pp}$ sine wave to the reference electrode, a small signal was immediately detected at the sensors. The signal grew as the reference electrode DC bias was decreased, and the EIS capacitor moved into the depletion regime. As the DC bias was decreased further and the capacitor entered accumulation, the signal leveled out at its peak value. Fig. 5.2a shows a CV curve taken by sweeping the DC bias of the reference electrode of device 5-27 (dual 80x80μm sensors) from 0V to –5V in increments of -10mV, while holding the sensors at 0V. The substrate bias was 2V.

Similar behavior was observed by applying increasingly larger positive DC offsets to the sensors while holding the reference electrode at 0V bias. Figure 5.2b shows a curve taken by sweeping the sensor bias levels in .1V increments. The reference electrode was held at a 0V bias, while the substrate bias was again 2V.

Several differences are apparent between the two curves. First, the maximum capacitance value of the top curve (reference electrode swept) is larger. Second, the threshold voltage between the two curves is different; the negative bias necessary at the reference electrode to reach the middle of the depletion curve is larger in magnitude than the positive sensor bias required to do the same. It was also observed that the sensors were less prone to drift when the sensors were biased, rather than the reference electrode.

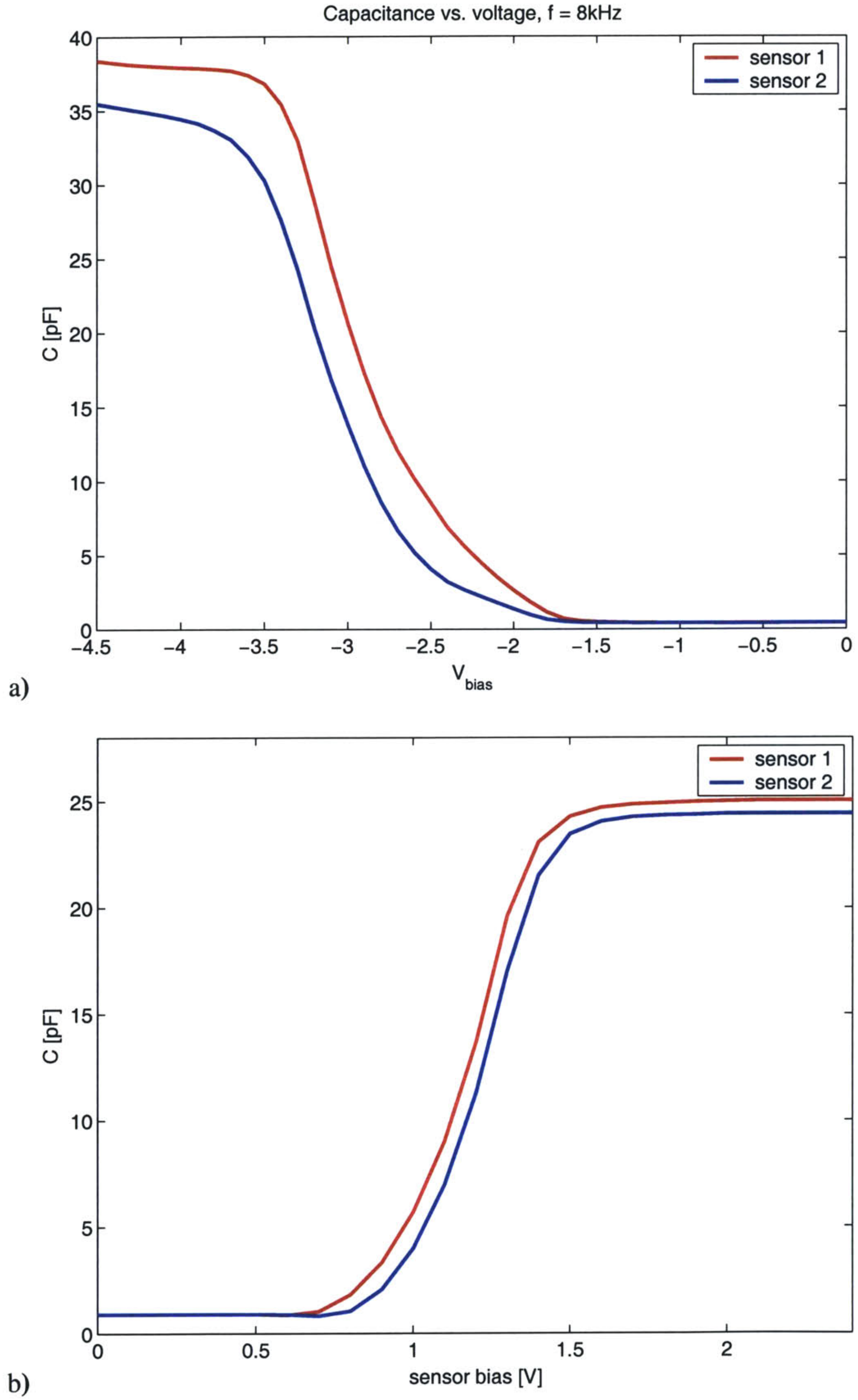

Fig. 5.2: Capacitance-voltage curves measured after injection of pH 7.44 phosphate buffer solution. (a) Bias voltage swept with reference electrode (b) Bias voltage swept with sensor bias control.

The maximum slope of the CV curve when the reference electrode is swept is approximately 44pF/V. For the CV curve taken by sweeping the sensor bias, the maximum slope is 30pF/V.

5.3.2 Sensitivity and noise performance

Device sensitivity was determined by biasing the sensors to the middle of the depletion curve and applying small potential increments while measuring the output response. A noise sample was then taken at the same bias voltage, and the root-mean-square (rms) noise levels were determined. The rms noise levels were then compared to the voltage steps to determine the smallest resolvable signal.

Noise performance was tested with device 5-27, with two 80x80μm sensor regions. The device was injected with pH 7.44 .01M PBS, and the sensors were individually biased to 1.10V. The device was equilibrated for approximately 30 minutes. Positive 2.5mV steps were first applied individually to the sensors, then a –2mV step was applied with the reference electrode (Fig. 5.3a). Next, a 55-second noise sample was recorded at the same bias voltage of 1.10V. As there was some drift during the noise collection period, the noise sample was leveled in MATLAB before the rms amplitude was determined. For both sensors on the chip, the rms noise floor was calculated:

Sensor	rms noise level
1	19μV
2	27.4μV

Table 5.4: Root-mean-square (rms) noise levels.

For these measurements, the lock-in amplifier output filter was set to a time constant of 100ms, with a 24dB/oct roll off. The noise floor was measured several more times, with results consistently below 30μV.

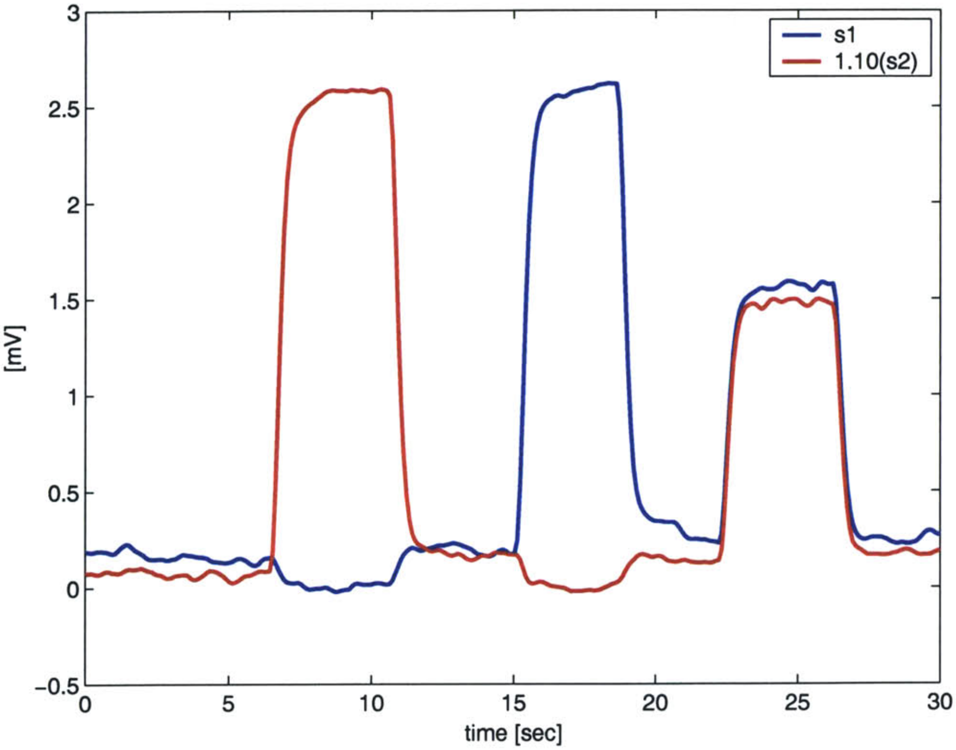

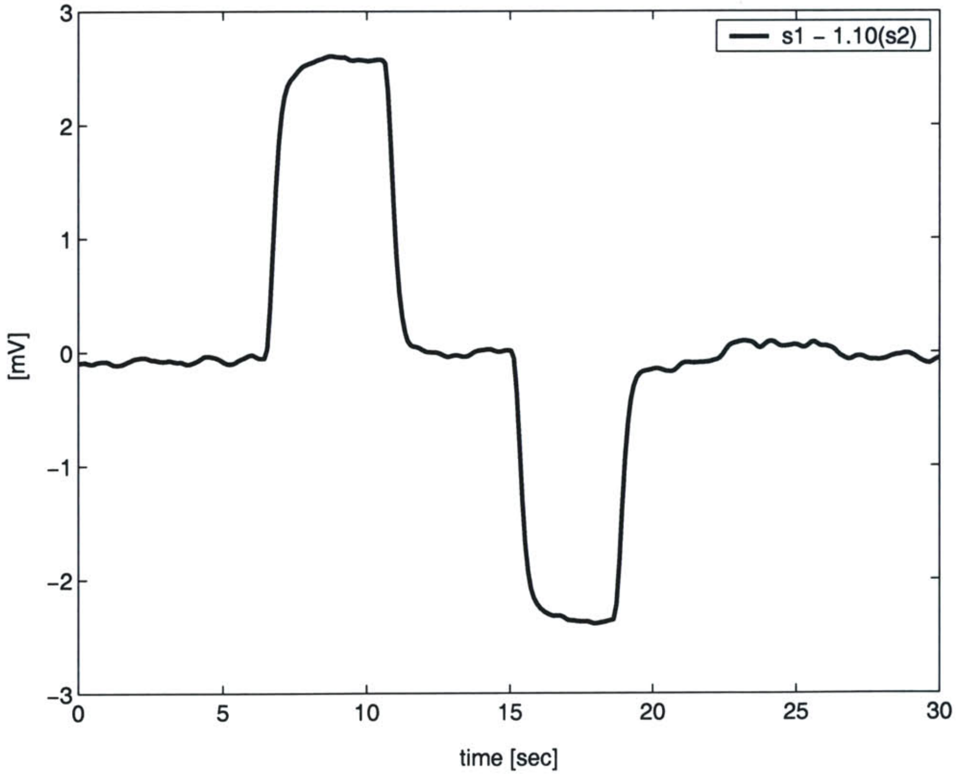

Fig. 5.3: (top) +2.5mV steps applied to sensors, then -2mV step applied to reference electrode. (bottom) Differential plot of top graph. Y-axis is references to 2.5mV step applied to sensor 1, Sensor 2 output is normalized by a factor of 1.10 to match sensor 1 output.

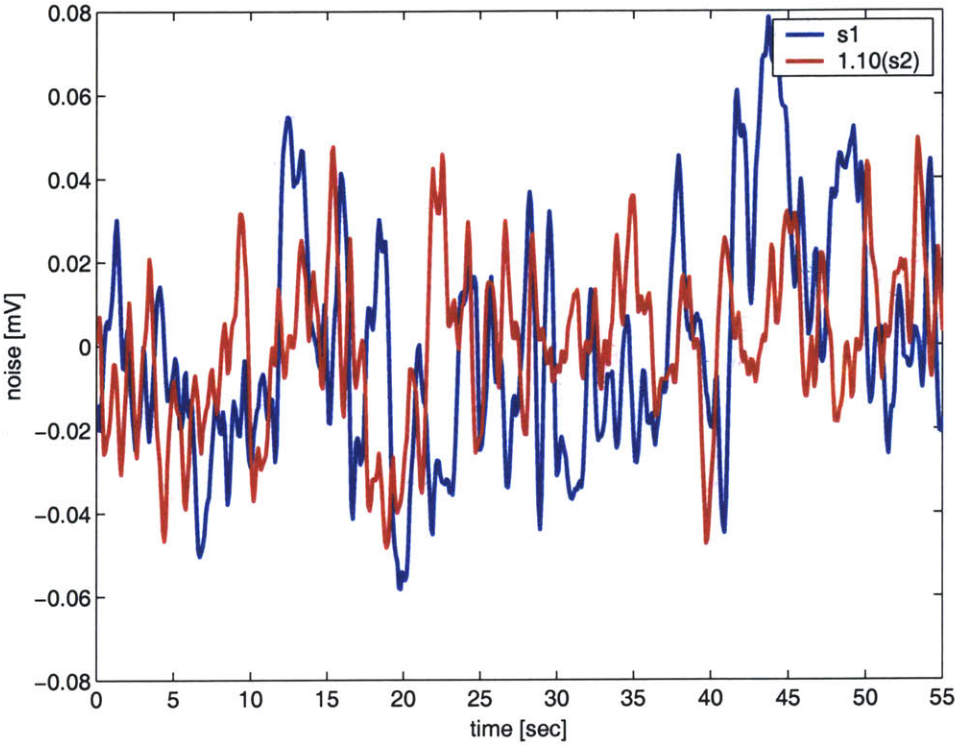

Fig. 5.4: Leveled and zeroed noise on sensors 1 and 2 with τ = 100ms filter.

5.3.3 pH response

Several experiments were conducted to measure the sensor's response to pH changes. To create a test solution of lower pH, 37% HCl was added in 5μL increments to 50mL .01M phosphate buffered saline, while the pH value was monitored with a meter. To create a test solution of higher pH value, 1M NaOH solution was first created by dissolving 2g NaOH pellets in 50mL Nanopure water. The NaOH solution was then added in 5μL increments to 50mL .01M PBS, and the pH was again monitored. The difference in ionic strength between the two new buffers and the stock PBS is negligible, as relatively small amounts of HCl and NaOH were added (less than .05% by volume).

During the initial testing, buffer solution was injected with a 50uL syringe, which was driven by a mechanical syringe pump. Between injections, the syringe was pulled from the tubing and refilled with a different solution. As discussed in section 5.1, the manual switching of fluids in this manner was problematic for several reasons.

In the experiment shown in Fig. 5.5, a dual 80x80μm device was used. The sensors were equilibrated with pH 6.36 PBS for one hour, with the reference electrode biased to -3.2V. Approximately twelve seconds into the experiment, pH 7.98 PBS was injected with a syringe pump, resulting in a rise in the output signal. Between 30 and 60 seconds, the syringe was removed from the PE input tube and refilled with pH 6.36 PBS. The second injection occurred at 63 seconds, at which point the signal decreased approximately to its initial value. At 75 seconds, positive and negative 40mV spikes were applied to the reference electrode to calibrate the output signals. The pH response in this experiment was 40mV/pH unit, referenced to the fluid bias electrode.

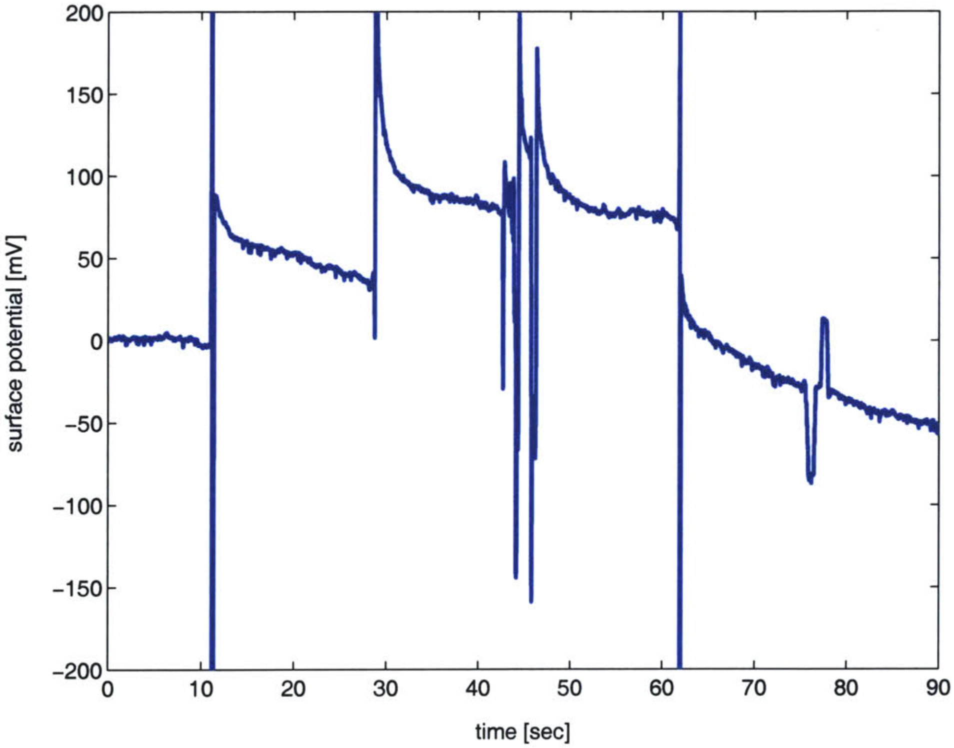

Figure 5.5: pH test with 80x80μm device. Initially, pH 6.36 PBS is present in device. At 12 seconds, pH 7.98 buffer was injected. At 63 seconds, pH 6.36 buffer was injected. pH response is approximately 40mV/decade, referenced to fluid bias electrode.

In the experiment shown in Fig. 5.6, the external fluid switching mechanism was used. pH 6.37 buffer was first injected into a type two (dual 50x50μm) device, and the device was allowed to equilibrate with both sensors biased to .72V. The buffer was replaced with pH 6.37 solution at 35 seconds into the experiment, and then the two solutions were switched several more times (see Fig. 5.6). Equivalent surface potential was determined by applying +/- 2.5mV pulses to each sensor and measuring the output signal. The pH response in this experiment was approximately 12mV/pH unit, referenced to the sensors.

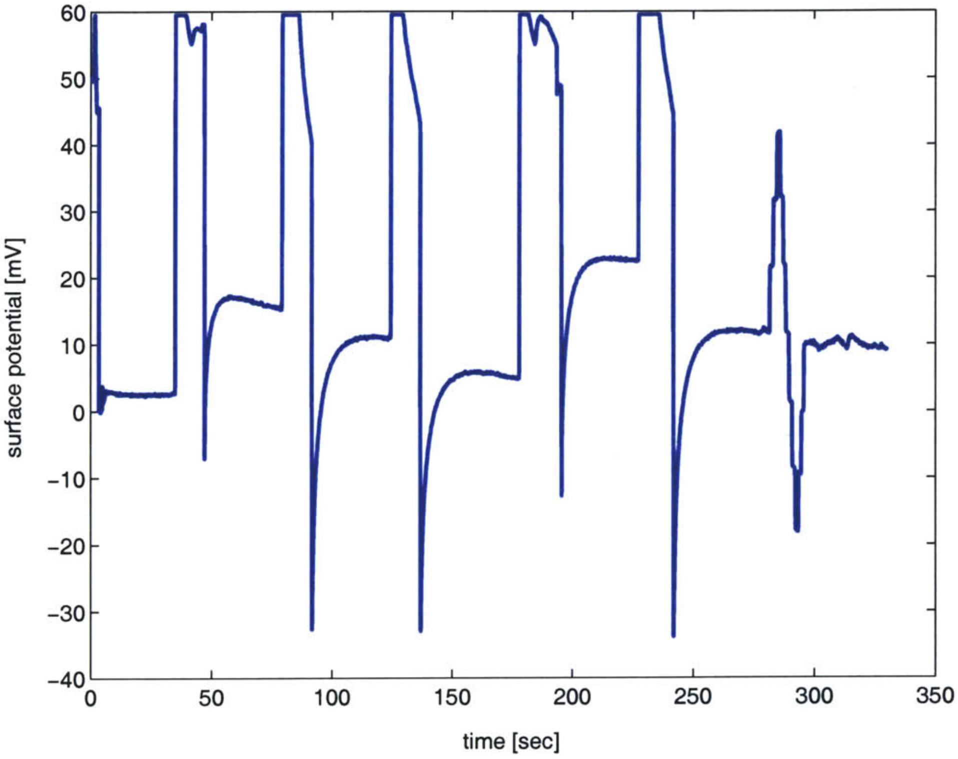

Fig. 5.6: pH test with 50x50μm device. Initially, device was equilibrated with pH 6.37 PBS. pH 7.44 buffer was injected at 35 seconds and 175 seconds. pH 6.37 buffer was injected at 80 seconds, 125 seconds, and 225 seconds. Response is approximately 12mV/decade, referenced to sensor bias.

6. FUTURE WORK AND CONCLUSIONS

6.1 Future work

There are several short-term goals for the development of the integrated field-effect sensors and microfluidics. One goal is to study the noise baseline of these devices in greater depth and compare it to that of other similar devices in the field, in particular nanowire detectors that have recently been reported [13].

Another short-term goal is to stack alternating layers of poly-l-lysine (PLL) and poly-l-glutamine (PLG) on the sensor surface and to detect the changes in surface potential. PLL is a positively charged polypeptide [9] that will bind to the oxide sensor surface, and PLG is a negatively charged molecule that will bind to the PLL. By repeatedly alternating the application of PLL and PLG to the sensor surface, positive and negative steps in surface potential may be observed. This experiment was shown in [9], and it is a nice demonstration of the capabilities of the sensors.

Currently, there is no cleaning method to strip the PLL/PLG layers once they have been applied to the sensor surface. Previous cantilever-based devices have been successfully dipped in BOE and Piranha between experiments. The devices in this paper will not withstand Piranha, however, as it will deteriorate the PDMS microfluidics. Other solvents, such as acetone, are readily absorbed by the PDMS. Thus, a new cleaning procedure must be developed that will not harm the microfluidics.

After demonstrating PLL/PLG layer stacking, single-stranded DNA sequences may be attached to the gate of the device with a PLL adhesion layer. Single-stranded complements to those sequences attached to the gate may then be applied. When binding occurs, the event may be detected by the sensors. This result has been shown in [9] and is another important step in validating the function of the sensors.

A future device enhancement is to integrate on-chip heating elements and microfluidic valves with the field-effect sensors. Such a system would enable on-chip polymerase chain reaction (PCR) amplification of DNA prior to field-effect detection. The current process flow (including the nitride field insulation) may readily be modified to include implanted heating coils. Valves compatible with the silicon layout have already been demonstrated, and are reported in Appendix C.

6.2 Conclusion

Integrated field-effect sensors and microfluidics for biomolecular detection have been demonstrated. The motivation for the development of field-effect biosensors is that they do not require the tagging of target molecules with fluorescent or radioactive tags prior to detection. The microfluidics enable measurements to be done with very small fluid samples. The integration of the two technologies forms a flexible micro total-analysis-system (μ-TAS) platform that may be used for a variety of biological assays.

This research has shown that multiple sensors and an integrated reference electrode may be included on the same chip with negligible leakage, by using p-type sensors in a heavily implanted n-type substrate. It has also demonstrated that nanoliter-scale volumes of fluid may be delivered directly to the sensors. The pH sensitivity and low noise baseline of the devices show promise for future development, including integrating on-chip valves, developing surface cleaning procedures, and detecting other types of charged molecules such as poly-l-lysine and DNA.

BIBLIOGRAPHY

1. Bedard, Daniel, Antimony L. Gerhardt, Trisha M. Montalbo, Peter R. Russo, Maxim Shusteff, Luke Theogarajan. "Integration of Microfluidics and Microelectronics: Enabling High Speed Sample Switching and pH Detection." 6.151 project report, M.I.T. (2002).

2. Bousse, L. "Single electrode potentials related to flat-band voltage measurements of EOS and MOS structures." *J. Chem. Phys.* **76**: 5128-5133 (1982).

3. Bergveld, P. "Development of an Ion-Sensitive Solid-State Device for Neurophysiological Measurements." *IEEE Transactions on Biomedical Engineering* **19**, No. 70 (1970).

4. Cooper, E.B., et al. "Robust microfabricated field-effect sensor for monitoring molecular absorption liquids." *Applied Physics Letters.* **79**, No. 23: 3875-3877 (2001).

5. Cooper, Emily Barbara. "Design, Fabrication, and Testing of a Scanning Probe Potentiometer." M.Eng. thesis, M.I.T. (2000).

6. Cooper, Emily Barbara. "Silicon Field-Effect Sensors for Biomolecular Assays." Ph.D. thesis, M.I.T. (2003).

7. Duffy, David C., et al. "Rapid prototyping of microfluidic switches in poly(dimethyl siloxane) and their actuation by electro-osmotic flow." *J. Micromech. Microeng.* **9**: 211-217 (1999).

8. Duffy, David C., et al. "Rapid Prototyping of Microfluidic Systems in Poly(dimethylsiloxane)." *Anal. Chem.* **70**: 4974-4984 (1998).

9. Fritz, Juergen, et al. "Electronic detection of DNA by its intrinsic molecular charge." *PNAS.* **99**, No. 22: 14142-14146 (2002).

10. Fu, A.Y., H.P. Chou, C. Spence, F.H. Arnold, S.R. Quake. "An Integrated Microfabricated Cell Sorter." *Anal. Chem.* (2002).

11. Gordon, B.J. "C-V Plotting: Myths and Methods." *Solid State Technology* **36**, No. 1: 57-61 (1993).

12. Howe, Roger T., and Charles G. Sodini. <u>Microelectronics: An Integrated Approach</u>. Prentice Hall (1997).

13. Li, Z., Y. Chen, X. Li, T.I. Kamins, R.S. Williams. "Sequence-Specific Label-Free DNA Sensors Based on Silicon Nanowires." To appear in *Nano Letters* (2004).

14. Loh, Nin C. "High-Resolution Micromachined Interferometric Accelerometer." S.M. thesis, M.I.T. (2001).

15. Manalis, S. R., et al. "Microvolume field-effect pH sensor for the scanning probe microscope." *Applied Physics Letters* **76,** No. 8: 1072-1074 (2000).

16. Sze, S.M. VLSI Technology, 2nd ed. McGraw-Hill, Inc. (1988).

17. Thorsen, T., S.J. Maerkl, S.R. Quake. "Microfluidic Large Scale Integration." *Science* **298**: 580-584 (2002).

18. Unger, M.A., H.P. Chou, T. Thorsen, A. Scherer, S.R. Quake. "Monolithic Microfabricated Valves and Pumps by Multilayer Soft Lithography." *Science* **288**: 113-116 (2000).

APPENDICES

A1. Detailed fabrication process flow

With the exception of the three ion implantation steps, fabrication of the integrated field-effect sensors and microfluidics was done at the M.I.T. Microsystems Technology Laboratories (MTL) cleanrooms. Process steps are labeled ICL, TRL, and EML, for the Integrated Circuits Laboratory (class 10), Technology Research Laboratory (class 100), and Exploratory Materials Laboratory (class 10,000), respectively.

Starting materials: 6” prime grade wafers, frontside polished. N-type (phosphorus doped), resistivity 20-50 Ω-cm, <100> orientation.

1. Pattern with global alignment mask (ICL, TRL)
On-track HMDS
Spin-cast 1.5μm SPR700-1.0 positive photoresist (2000 rpm, 30sec)
On-track prebake
Expose with EV1 mask aligner, 5sec
Develop with AZ440MIF, 20-25sec
DI water rinse, spin dry
Postbake at 120C°, 30min

2. Etch global alignment marks (ICL)
LAM490 plasma etcher
Black silicon recipe, 2:30 etch time

3. Ash photoresist (ICL)
Matrix 106 asher, 3min

4. Clean wafers with Piranha (ICL)
3:1 H_2SO_4 : H_2O_2, 15min
DI water rinse, spin dry

5. RCA clean (ICL)
5:1:1 H_2O : H_2O_2 : NH_4OH, 10min
DI water rinse
50:1 H_2O : HF, 15sec
DI water rinse
6:1:1 H_2O : H_2O_2 : HCl, 15sec
DI water rinse, spin dry

6. 30nm thermal SiO_2 (ICL)
Dry O_2 oxidation at 950°C
Tube 5A-GateCMOS
1D950 recipe, 60min variable time

7. Pattern with p+ (connecting traces) implant mask (ICL, TRL)
On-track HMDS
Spin-cast 1.5μm SPR700-1.0 positive photoresist (2000 rpm, 30sec)
On-track prebake
Expose with EV1 mask aligner, 5sec
Develop with LDD-26W, 60sec
DI water rinse, spin dry
Postbake at 120°C, 30min

8. Ion implantation
Implant Sciences Corporation, Wakefield, MA
Species: Boron
Dose: $2 \cdot 10^{15}$ cm^{-2}
Energy: 150keV

9. Clean and strip photoresist (TRL)
Piranha (3:1 H_2SO_4 : H_2O_2), 20min
DI water rinse
Piranha (3:1 H_2SO_4 : H_2O_2), 20min
DI water rinse, spin dry

10. Pattern with p (sensor regions) implant mask (ICL, TRL)
On-track HMDS
Spin-cast 1.5μm SPR700-1.0 positive photoresist (2000 rpm, 30sec)
On-track prebake
Expose with EV1 mask aligner, 5sec
Develop with LDD-26W, 60sec
DI water rinse, spin dry
Postbake at 120°C, 30mins

11. Ion implantation
Implant Sciences Corporation, Wakefield, MA
Species: Boron
Dose: $2 \cdot 10^{11}$ cm^{-2}
Energy: 200 keV

12. Clean and strip photoresist (TRL)
20min Piranha (3:1 H_2SO_4 : H_2O_2)
DI water rinse
20min Piranha (3:1 H_2SO_4 : H_2O_2)
DI water rinse, spin dry

13. Pattern with n+ (substrate) implant mask (ICL, TRL)
On-track HMDS
Spin-cast 1.5μm SPR700-1.0 positive photoresist (2000 rpm, 30sec)
On-track prebake
Expose with EV1 mask aligner, 4.5sec
Develop in LDD-26W, 60sec
DI water rinse, spin dry
Postbake at 120° C, 30mins

14. Ion implantation
Implant Sciences Corporation, Wakefield, MA
Species: Phosphorus
Dose: 10^{15} cm^{-2}
Energy: 200keV

15. Clean and strip photoresist (TRL)
20min Piranha (3:1 H_2SO_4 : H_2O_2)
DI water rinse
20min Piranha (3:1 H_2SO_4 : H_2O_2)
DI water rinse, spin dry

16. Buffered Oxide Etch
7:1 HF : H_2O, 60sec
DI water rinse, spin dry

17. RCA clean (ICL)
5:1:1 H_2O : H_2O_2 : NH_4OH, 10min
DI water rinse
50:1 H_2O : HF, 15sec
DI water rinse
6:1:1 H_2O : H_2O_2 : HCl, 15sec
DI water rinse, spin dry

18. 50nm thermal SiO_2 (ICL)
Dry O_2 oxidation at 950°C
Tube 5A-GateCMOS, 1D950 recipe, 60min variable time
Measured thickness with UV1280: 53nm

19. 1μm Si_3N_4 deposition (ICL)
Vertical Thermal Reactor (VTR) deposition
Measured thickness with UV1280: 1.03μm

20. Dopant drive-in (ICL)
Inert anneal, 1050 °C
Tube 5B-Anneal, 240min variable time

21. Pattern with contacts mask (ICL, TRL)
On-track HMDS
Spin-cast 1.5μm SPR700-1.0 positive photoresist (2000 rpm, 30sec)
On-track prebake
Expose with EV1 mask aligner, 4.5sec
Develop in LDD-26W, 60sec
DI water rinse, spin dry
Postbake at 120°C, 30mins

22. Etch nitride (ICL)
Applied Materials AME5000 plasma etcher
NITRIDE CF4 recipe, 3:30 etch time
Measured etch depth with profilometer: 1.08-1.09μm at center

23. Ash photoresist (ICL)
Matrix 106 asher, 4mins

21. Pattern frontside with metal mask (ICL, TRL)
Wafers heated in HMDS oven, no cycle run
Spin cast 2 μm image reversal negative photoresist (1500 rpm, 30sec)
Prebake at 95°C, 30mins
Expose with EV1 mask aligner, 2.0sec
Bake at 95°C, 35mins
Flood expose with EV1 mask aligner, 45sec
Develop in AZ422, 2mins
DI water rinse, spin dry

22. Ash photoresist (TRL)
5mins in TRL asher at 1000W
"Descum" step prior to metal deposition

23. Buffered Oxide Etch (TRL)
7:1 HF : H_2O, 30sec
DI water rinse, spin dry

24. Metal evaporation (TRL)
20nm titanium, 1000nm gold

25. Metal lift-off (TRL)
Overnight soak in acetone
Spray with methanol
DI water rinse, dry with air gun

26. Coat frontside with photoresist (TRL) & die-sawing (ICL)

A2. SUPREM simulation code

```
$ setup grid
LINE X LOC=0 SPAC=.2
LINE X LOC=25 SPAC=.2
LINE Y LOC=0 SPAC=.05
LINE Y LOC=2 SPAC=.05

$ start with <100> n-type wafer
$ INIT <100> PHOSPHORUS=4E14
INIT <100> IMPURITY=phosphorus I.RESIST=20

$ thin oxide
DIFFUSION TEMP=950 TIME=60 DRYO2
EXTRACT OXIDE X=0 THICKNES

$ p+ implant
DEPOSITION PHOTORES THICKNES=1.5
ETCH PHOTORES START X=10 Y=0
ETCH CONTINUE X=20 Y=0
ETCH CONTINUE X=20 Y=-2
ETCH DONE X=10 Y=-2
IMPLANT BORON DOSE=2e15 ENERGY=150 TILT=7

ETCH PHOTORES ALL

$ p implant
DEPOSITION PHOTORES THICKNES=1.5
ETCH PHOTORES START X=15 Y=0
ETCH CONTINUE X=25 Y=0
ETCH CONTINUE X=25 Y=-2
ETCH DONE X=15 Y=-2
IMPLANT BORON DOSE=2e11 ENERGY=200 TILT=7

ETCH PHOTORES ALL

$ n+ implant
DEPOSITION PHOTORES THICKNES=1.5
ETCH PHOTORES START X=0 Y=0
ETCH CONTINUE X=5 Y=0
ETCH CONTINUE X=5 Y=-2
ETCH DONE X=0 Y=-2
IMPLANT PHOSPHORUS DOSE=1e15 ENERGY=200 TILT=7

ETCH PHOTORES ALL

ETCH OXIDE ALL

$ thin pad oxide
$ target ~ 50nm
DIFFUSION TEMP=1000 TIME=60 DRYO2

EXTRACT OXIDE X=2.5 THICKNES
EXTRACT OXIDE X=15 THICKNES
EXTRACT OXIDE X=22.5 THICKNES
```

```
DEPOSITION NITRIDE THICKNES=1

$ dopant anneal
DIFFUSION TEMP=1050 TIME=240 INERT

OPTION device=ps-c file.sav=n+.ps
SELECT Z=LOG10(PHOSPHORUS)
PLOT.1D X.VALUE=2.5 LINE.TYP=1 COLOR=2
SELECT Z=LOG10(DOPING)
PLOT.1D X.VALUE=2.5 ^AXES ^CLEAR LINE.TYP=1 COLOR=5

SELECT Z=PHOSPHORUS
PRINT.1D X.VALUE=2.5 OUT.FILE=phos2.5.dat
SELECT Z=DOPING
PRINT.1D X.VALUE=2.5 OUT.FILE=doping2.5.dat

OPTION device=ps-c file.sav=n.ps
SELECT Z=LOG10(PHOSPHORUS)
PLOT.1D X.VALUE=7.5 ^AXES ^CLEAR LINE.TYP=1 COLOR=2
SELECT Z=LOG10(DOPING)
PLOT.1D X.VALUE=7.5 ^AXES ^CLEAR LINE.TYP=1 COLOR=5

OPTION device=ps-c file.sav=p+.ps
SELECT Z=LOG10(BORON)
PLOT.1D X.VALUE=12.5 LINE.TYP=1 COLOR=4
SELECT Z=LOG10(PHOSPHORUS)
PLOT.1D X.VALUE=12.5 ^AXES ^CLEAR LINE.TYP=1 COLOR=2
SELECT Z=LOG10(DOPING)
PLOT.1D X.VALUE=12.5 ^AXES ^CLEAR LINE.TYP=1 COLOR=5

SELECT Z=BORON
PRINT.1D X.VALUE=12.5 OUT.FILE=boron12.5.dat
SELECT Z=PHOSPHORUS
PRINT.1D X.VALUE=12.5 OUT.FILE=phos12.5.dat
SELECT Z=DOPING
PRINT.1D X.VALUE=12.5 OUT.FILE=doping12.5.dat

OPTION device=ps-c file.sav=pp+.ps
SELECT Z=LOG10(BORON)
PLOT.1D X.VALUE=17.5 LINE.TYP=1 COLOR=4
SELECT Z=LOG10(PHOSPHORUS)
PLOT.1D X.VALUE=17.5 ^AXES ^CLEAR LINE.TYP=1 COLOR=2
SELECT Z=LOG10(DOPING)
PLOT.1D X.VALUE=17.5 ^AXES ^CLEAR LINE.TYP=1 COLOR=5

OPTION device=ps-c file.sav=p.ps
SELECT Z=LOG10(BORON)
PLOT.1D X.VALUE=22.5 LINE.TYP=1 COLOR=4
SELECT Z=LOG10(PHOSPHORUS)
PLOT.1D X.VALUE=22.5 ^AXES ^CLEAR LINE.TYP=1 COLOR=2
SELECT Z=LOG10(DOPING)
PLOT.1D X.VALUE=22.5 ^AXES ^CLEAR LINE.TYP=1 COLOR=5

SELECT Z=BORON
PRINT.1D X.VALUE=22.5 OUT.FILE=boron22.5.dat
SELECT Z=PHOSPHORUS
PRINT.1D X.VALUE=22.5 OUT.FILE=phos22.5.dat
```

```
SELECT Z=DOPING
PRINT.1D X.VALUE=22.5 OUT.FILE=doping22.5.dat

OPTION device=ps-c file.sav=lateral.ps
SELECT Z=LOG10(DOPING)
PLOT.2D X.MIN=0 X.MAX=25 Y.MAX=3 LINE.TYP=2
COLOR MATERIAL=SILICON COLOR=1
COLOR MATERIAL=OXIDE COLOR=5
FOREACH X (15 TO 20 STEP .5)
COLOR MIN.VALUE=X MAX.VALUE=(X + .5) COLOR=((2 * (X - 15)) + 8)
```

A3. PDMS air-actuated valves

PDMS air-pressure actuated valves (based on those developed by Quake, et. al; see [17, 18]) that are compatible with the field-effect sensor chips have been fabricated. Air actuated valves consist of two layers of bonded PDMS; the bottom layer contains the microfluidic channels, while the top layer contains the air channels. The microfluidic channels may be pinched off in certain points by pressurizing the appropriate air channels above. The valves that were constructed in lab require air pressures of 12 – 15psi for activation. The valvs

Fabrication of PDMS valves is almost identical to the construction of regular microfluidic channels (see section 4.3). First, a fluidics mold wafer was created. However, rather than SU-8, thick positive photoresist (AZ4620) was used. After being treated with HMDS in a vapor prime oven, a wafer was spin-coated with approximately 10 microns of AZ4620. After a short pre-bake, the wafer was exposed to a light-field transparency mask and developed. Next, the photoresist was reflowed at 200°C for 30 minutes. Reflowing the photoresist creates an easily compressible semicircular cross-sectional profile:

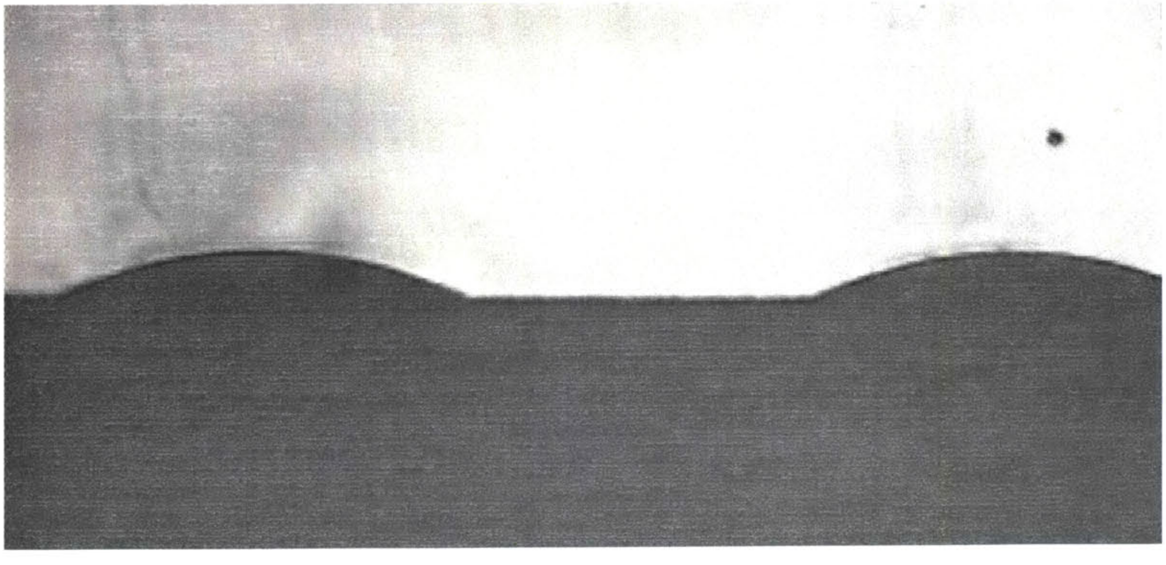

Fig. A1: Cross-section of PDMS (white) showing rounded channel profile.
Channel width = 100μm, maximum height = 10μm.

After reflowing the photoresist, the wafer was vacuum treated with (tridecafluoro-1,1,2,2-tetrahydrooctyl)-1-trichlorosilane to ease the removal of PDMS.

Rather than casting PDMS over the wafer, PDMS was spin-coated at 1000rpm for 30 seconds, resulting in a thin PDMS film approximately 40 microns thick. The film was cured for 30 minutes at 80°C. The upper air layer was fabricated in the usual way, using SU-8 and a dark-field photomask to created a mold wafer, and the PDMS was cast. After dicing the top layer, a top layer die and the entire bottom layer film (left spin-coated on the fluidics master wafer) were plasma treated, aligned, and bonded. An alignment jig made of a Newport translation stage and laser-cut acrylic adapters was precise to within approximately 10μm.

Given the time constraints of this thesis project, it was not possible to test a sensor with integrated PDMS valves. However, this remains a high priority for future project development.

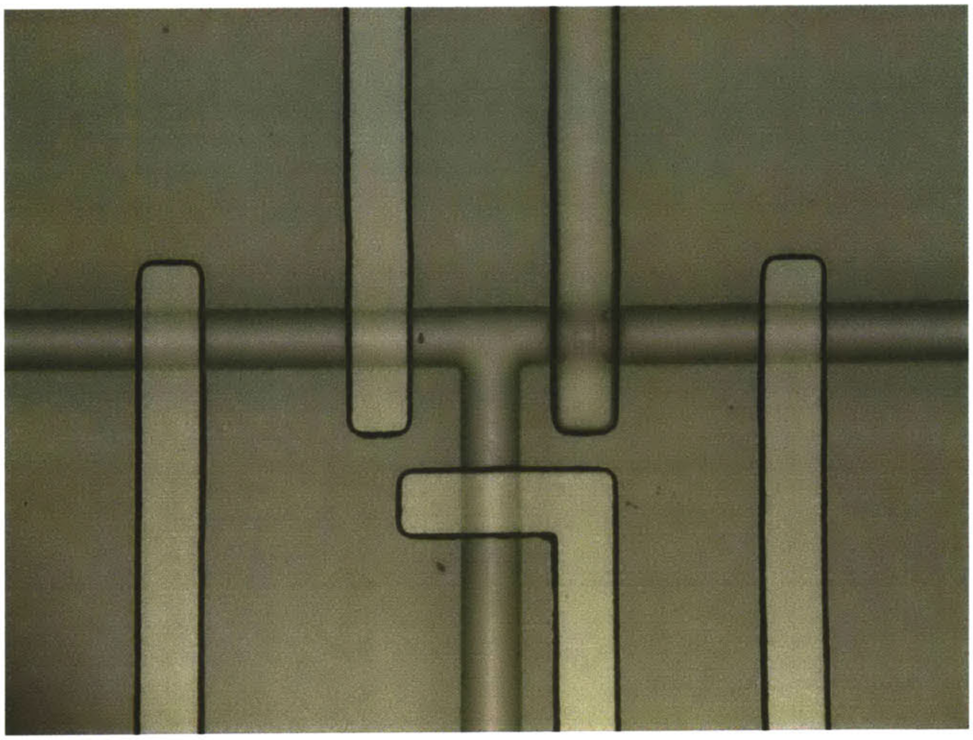

Fig. A2: T-shaped microfluidic channels and five overlayed valves.

6075-47